



140
429
THS

1
2007

This is to certify that the
thesis entitled

DIAMOND OPTICALLY TRANSPARENT ELECTRODES FOR
USE IN IR TRANSMISSION SPECTROELECTROCHEMICAL
MEASUREMENTS

presented by

Yingrui Dai

has been accepted towards fulfillment
of the requirements for the

 M.S. degree in Chemistry

 Greg M. Swain
Major Professor's Signature

 May 10, 2007

Date

MSU is an affirmative-action, equal-opportunity employer

LIBRARY
Michigan State
University

PLACE IN RETURN BOX to remove this checkout from your record.
TO AVOID FINES return on or before date due.
MAY BE RECALLED with earlier due date if requested.

DATE DUE	DATE DUE	DATE DUE

**DIAMOND OPTICALLY TRANSPARENT ELECTRODES
FOR USE IN IR TRANSMISSION
SPECTROELECTROCHEMICAL MEASUREMENTS**

By

Yingrui Dai

A THESIS

Submitted to
Michigan State University
in partial fulfillment of the requirements
for the degree of

MASTER OF SCIENCE

Department of Chemistry

2007

ABSTRACT

DIAMOND OPTICALLY TRANSPARENT ELECTRODES FOR USE IN IR TRANSMISSION SPECTROELECTROCHEMICAL MEASUREMENTS

By

Yingrui Dai

The goal of the research was to develop boron-doped diamond optically transparent electrodes for use in the IR transmission spectroelectrochemical measurements. The diamond film was deposited by microwave-assisted chemical vapor deposition for 4 h using a 0.5% CH₄/H₂ with 2 ppm B₂H₆ source gas mixture at 45 torr and 1000 W. The diamond/Si OTE transmits approximately 40-60% of IR light (2000-700 cm⁻¹). SEM, Raman spectroscopy and XRD results confirmed the presence of a thin, high quality boron-doped diamond film. The low film resistivity (0.1-0.4 Ω-cm) and good electrode activity produced relatively rapid electron-transfer reaction kinetics for both aqueous (Fe(CN)₆^{-3/-4}, methyl viologen, Ru(NH₃)₆^{+3/+2} and IrCl₆^{-2/-3}) and non-aqueous (ferrocene) redox couples. Difference FTIR spectra (oxidized minus reduced) for 10 mM Fe(CN)₆^{-3/-4} in 1 M KCl recorded at various applied potentials showed that the CN vibrational mode at 2039 cm⁻¹ for Fe(CN)₆⁻⁴ reversibly shifted upon oxidation to 2116 cm⁻¹ as expected. From the difference FTIR spectra of 20 mM ferrocene in 0.1 M TBABF₄/CH₃CN, the shift of the C-H bending mode perpendicular to the plane of the cyclopentadienyl ring from 823 cm⁻¹ to 857 cm⁻¹ showed the conversion of the ferrocene to the ferricenium ion. The results showed that the diamond/Si OTE possesses good electrical conductivity and optical transparency enabling rapid, reproducible and quantitative spectroelectrochemical measurements in the mid- and far- IR.

ACKNOWLEDGEMENTS

The past three years at Michigan State University is a valuable experience in my life. I have learned a lot: how to be a researcher, how to drive, and how to love.

The first person I want to thank is my advisor, Dr. Greg Swain. Thanks for his guidance and encouragement over the last three years. I have been fortunate to work with Dr. Jerzey Zak and Dr. Denis A. Proshlyakov. I thank you sincerely for helping me develop the skills critical to being a scientist through the discussions. Thanks to my committee members, Dr. Gary Blanchard, and Dr. David Weliky for your helpful comments about my work. I have never had the opportunity to work with a welcoming, encouraging group of people in the Swain Lab. Words alone can not express my gratefulness to Elizabeth, Yang, Shihua, Anne, Jason, Veronika, Martin, Dasa, Luther; Matt, Isao, Ayten and Aihua. You guys are the best.

I also want to thank my best friends: Xin, Xiaoyu, Chang and Meng. It is nice to have you in my life that saw me through the process. You always show up when I need you. That is a friend indeed.

Finally, and most importantly, I would like to say thank you to my parents and liangxing. Without your love and support, I would not be here today. Thank you for always being there with me. Love you forever.

TABLE OF CONTENTS

List of Tables	vi
List of Figures	vii
CHAPTER 1 – Introduction	1
1.1 Spectroelectrochemistry.....	1
1.2 Optically Transparent Electrodes (OTE)	4
1.3 Development of Optically Transparent Boron-Doped Diamond Electrode.....	6
1.3.1 Boron-Doped Diamond Electrode.....	6
1.3.2 Optically Transparent Boron-Doped Diamond Electrode.....	7
1.4 Outline of Thesis.....	10
1.5 References.....	11
CHAPTER 2 – Experimental Methods	14
2.1 Diamond Thin Film Deposition.....	14
2.2 Material Characterization.....	16
2.2.1 Scanning Electron Microscopy (SEM).....	16
2.2.2 Raman Spectroscopy.....	16
2.2.3 X-Ray Diffraction Spectroscopy (XRD)	17
2.2.4 Four-Point Probe Measurements.....	17
2.2.5 Optical Transmission Measurements.....	18
2.2.6 Electrochemical Characterization.....	18
2.3 Spectroelectrochemical Measurements.....	20
2.3.1 Thin-Layer Spectroelectrochemical Cell.....	20
2.3.2 Potential Step Method.....	22
2.3.3 Temperature Control.....	23
2.4 Chemicals.....	24
2.5 References.....	25
CHAPTER 3 – Optical, Electrical, Physical and Electrochemical Properties of the Boron-Doped Diamond Electrodes	26
3.1 Introduction	26
3.2 Results and Discussion.....	29
3.2.1 Optical Properties of Diamond/Si OTE-IR.....	29
3.2.2 Electrical Properties of Diamond/Si OTE.....	32
3.2.3 Physical Properties of Diamond/Si OTE.....	33

3.2.4 Electrochemical Properties of Diamond OTE.....	36
3.3 Conclusions.....	45
3.4 References.....	47

CHAPTER 4 – IR Transmission Spectroelectrochemical Measurements With an Optically Transparent Boron-Doped Diamond Electrode.....49

4.1 Introduction.....	49
4.2 Results and Discussion.....	52
4.3 Conclusions.....	61
4.4 References.....	63

CHAPTER 5 – Key Findings and Perspectives.....64

5.1 Conclusions.....	64
5.2 Future Research Directions.....	66
5.2.1 Metalloproteins.....	66
5.2.2 Far-IR Spectroelectrochemical Measurements of Redox Metalloproteins....	67

LIST OF TABLES

Table 3-1	Effect of growth parameters on the properties of diamond/Si OTE.....	28
Table 3-2	Comparison between measured XRD data for a diamond/Si OTE and values from ASTM (6-0675) cubic diamond standard.....	36
Table 3-3	Summary of cyclic voltammetric data for diamond/Si OTEs deposited for 4 h using 2 ppm B ₂ H ₆ . The scan rate was 0.1 V/s.....	40
Table 3-4	Concentration dependence of the cyclic voltammetric data at a diamond/Si OTE.....	44
Table 3-5	Scan rate dependence of the cyclic voltammetric data at a diamond/Si OTE.....	45

LIST OF FIGURES

- Figure 1-1** Difference types of spectroelectrochemical techniques.....2
- Figure 1-2** Two conventional OTEs for transmission measurements: (A) a metal minigrad and (B) a thin film supported on an optically transparent substrate.....4
- Figure 1-3** Schematic of bonding arrangement of sp^3 -bonded diamond.....6
- Figure 2-1** A schematic of a microwave plasma-assisted CVD reactor used to grow boron-doped diamond thin-film electrodes.....14
- Figure 2-2** Design of the single-compartment, three-electrode electrochemical cell with (a) the diamond film working electrode, (b) O-ring seal, (c) nickel foil and rubber spacer, (d) reference electrode inside a glass capillary tube with a cracked tip, (e) carbon rod counter electrode, and (f) input for nitrogen purge gas.....19
- Figure 2-3** Diagram of the IR transmission thin-layer spectroelectrochemical cell.....21
- Figure 2-4** Potential-time profile for the recording of spectroelectrochemical measurements. An absorbance spectrum was recorded at each potential as indicated by the arrows.....22
- Figure 2-5** Principle of absorbance difference spectroscopy.....23
- Figure 3-1** IR transmission spectra for different types of boron-doped diamond electrodes: (A) a CVD “white” (type IIa) diamond disc, (B) undoped and polished Si substrate, (C) boron-doped diamond thin film deposited on the undoped Si using 2 ppm B_2H_6 and 4-h growth time, (D) boron-doped diamond thin film deposited on the undoped Si using 5 ppm B_2H_6 and 4-h growth time, and (E) boron-doped diamond thin film deposited on the undoped Si using 2 ppm B_2H_6 and a 10-h growth time.....30
- Figure 3-2** IR absorption spectrum of boron-doped diamond/Si OTE deposited for 4 h using 2 ppm B_2H_631
- Figure 3-3** Four-point probe electrical resistivity measurements for five different diamond/Si OTEs deposited for 4 h using 2 ppm B_2H_632

- Figure 3-4** Scanning electron micrographs of a diamond/Si OTE: (A) top view (B) side section view. The film was deposited for 4 h using 2 ppm B₂H₆.....33
- Figure 3-5** Raman spectrum for a diamond/Si OTE deposited for 4 h using 2 ppm B₂H₆.....34
- Figure 3-6** Powder X-ray diffraction spectrum of a diamond/Si OTE deposited for 4 h using 2 ppm B₂H₆.....36
- Figure 3-7** Cyclic voltammetric *i-E* curve in 1 M KCl for a diamond/Si OTE deposited for 4 h using 2 ppm B₂H₆. Scan rate = 0.1 V/s.....37
- Figure 3-8** Cyclic voltammetric *i-E* curves for 0.1 mM Fe(CN)₆^{-3/-4}, methyl viologen, Ru(NH₃)₆^{+3/+2} and IrCl₆^{-2/-3}, all in 1 M KCl, at a diamond/Si OTE deposited for 4 h using 2 ppm B₂H₆. Scan rate = 0.1 V/s. Electrode geometric area = 0.2 cm².....39
- Figure 3-9** Cyclic voltammetric *i-E* curve for 0.1 mM ferrocene in 0.1 M TBABF₄/CH₃CN at a diamond/Si OTE deposited for 4 h using 2 ppm B₂H₆. Scan rate = 0.1 V/s. Electrode geometric area = 0.2 cm².....39
- Figure 3-10** Cyclic voltammetric *i-E* curves for 0.05, 0.1, 0.5, and 1mM (A) Fe(CN)₆^{-3/-4}, (B) Ru(NH₃)₆^{+3/+2}, (C) IrCl₆^{-2/-3}, and (D) methyl viologen, all in 1 M KCl, with a diamond/Si OTE deposited for 4 h with 2 ppm B₂H₆. Scan rate = 0.1 V/s. Electrode geometric area = 0.2 cm².....43
- Figure 4-1** Cyclic voltammetric data for the diamond/Si OTE with 7.5 μm spacer. (A) Background-corrected thin-layer cyclic voltammetric *i-E* curve for 1 mM Fe(CN)₆⁻⁴ in 1 M KCl. The scan rate was 1 mV/s. (B) Plots of the oxidation (square) and reduction (triangular) peak current vs. scan rate for 1 mM Fe(CN)₆⁻⁴ in 1 M KCl. Data are shown for scan rates from 1 to 5 mV/s....53
- Figure 4-2** IR spectroelectrochemical difference absorbance spectra of Fe(CN)₆^{-3/-4} at the diamond/Si OTE with a CaF₂ window. The optical pathlength was 7.5 μm. The analyte solution was 10 mM Fe(CN)₆⁻⁴ in 1 M KCl. The potential was stepped from 0 to 0.1 V, 0.2 V, 0.25 V, 0.3 V, 0.35 V, 0.4 V, and 0.5 V vs. Ag/AgCl. Each spectrum was generated by subtracting the reference spectrum obtained at 0 V.....55
- Figure 4-3** Nernst plots for 10 mM Fe(CN)₆⁻⁴ in 1 M KCl. (A) the Fe(CN)₆⁻⁴ absorption at 2039 cm⁻¹ and (B) the Fe(CN)₆⁻³ absorption at 2116 cm⁻¹. Plots were

generated from spectroelectrochemical data obtained with a diamond/Si OTE as presented in Figure 4-2.....57

Figure 4-4 IR spectroelectrochemical absorbance spectra for $\text{Fe}(\text{CN})_6^{-4}$ (solid line) and electrogenerated $\text{Fe}(\text{CN})_6^{-3}$ (dashed line) at the diamond/Si OTE with a CaF_2 window. The optical pathlength was 7.5 μm . The analyte solution was 10 mM $\text{Fe}(\text{CN})_6^{-4}$ in 1 M KCl. Oxidized minus reduced (dashed line) and reduced minus oxidized (solid line) spectra were generated from the oxidized and reduced spectra collected at 0.5 and 0 V during a forward and reverse potential step for 60 s.....58

Figure 4-5 Difference absorbance-potential curves for $\text{Fe}(\text{CN})_6^{-3/4}$ at the diamond/Si OTE with a CaF_2 window. The optical pathlength was 7.5 μm . The measurement was made for a solution of 10 mM $\text{Fe}(\text{CN})_6^{-4}$ in 1 M KCl. The data were collected at a scan rate of 2 mV/s. The IR spectra were collected within a range of wavenumbers during the scanning, the final difference absorbance at each potential was actually an average of a small range of potential.....60

Figure 4-6 IR spectroelectrochemical difference absorbance spectra of ferrocene at the diamond/Si OTE with a Si window. The optical pathlength was 75 μm . The analyte solution was 20 mM ferrocene in 0.1 M $\text{TBABF}_4/\text{CH}_3\text{CN}$. The potential was stepped from 0.1 to 0.9 V vs. Pt-QRE in increments of 0.1 V. Each spectrum was generated by subtracting the reference spectrum for the fully reduced form at 0.1 V.....61

CHAPTER 1

Introduction

1.1 Spectroelectrochemistry

Spectroelectrochemistry is a hybrid of two techniques: spectroscopy and electrochemistry. The technique (transmission mode) can be used to record the change in the spectroscopic signature of an analyte associated with a change in redox state brought about by electron transfer with an optically transparent electrode (OTE). It provides more information about a redox reaction mechanism than that can be acquired using traditional electrochemical methods alone. Spectroelectrochemistry has been used for nearly 40 years in the study of inorganic, organic, and biological redox systems.^{1,2}

Considerable development in spectroelectrochemistry has taken place since its inception in 1964 when Kuwana introduced this hybrid analytical method.³ The coupling of a variety of spectroscopic and electrochemical techniques has enabled new and powerful combinations to be applied to complex redox systems.⁴⁻⁶ In fact, spectroelectrochemistry has been used with electromagnetic radiation from almost every region of the electromagnetic spectrum.^{2, 7, 8} Some commonly used spectroscopic methods that have been coupled with electrochemistry are listed in Figure 1-1.

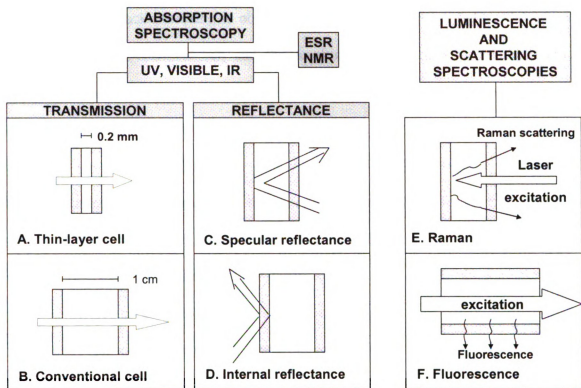


Figure 1-1 Different types of spectroelectrochemical techniques. (adapted with permission from references 8)

Absorption spectroscopy in the ultraviolet, visible, or infrared regions is most often employed. In the transmission mode (Figure 1-1 A, B), the optical beam is directed orthogonally through an OTE and the adjacent solution layer. Specular reflectance spectroscopy (Figure 1-1, C) involves passing light through a solution layer and measurement of the light reflected from the electrode surface. In the internal reflection mode (Figure 1-1, D), the light beam is introduced through the back side of an OTE at an angle greater than the critical angle so that the beam is totally internally reflected. The light interacts with species present adjacent to the electrode surface. The sensitivity can be increased by causing multiple reflections to occur. In normal and resonance Raman spectroscopy (Figure 1-1, E), a laser beam is directed through the solution at an electrode

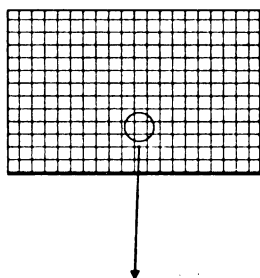
and the Raman back-scattering is observed. A beam of excitation light can be passed through an electrochemical cell and the resulting luminescence by electrogenerated species can be recorded (Figure 1-1, F). Many other techniques, such as, surface plasmon resonance (SPR), mass spectrometry (MS), electron spin resonance (EPR), nuclear magnetic resonance (NMR), X-ray diffraction (XRD), have also been coupled with electrochemistry. In summary, the transmission mode provides information about the electrochemical reaction in the solution, the reflectance mode is more focused on the electrode/electrolyte interface, and the scattering mode is useful for the investigation of electrogenerated species adsorbed on the electrode surface.

The most frequently used spectroelectrochemical measurement mode is the transmission one through a thin-layer cell. One of the main advantages of the thin-layer cell design is that the electroactive analyte present can be exhaustively electrolyzed in a very short time (typically 20-120 s depending on the cell thickness). In the design, there is finite diffusion, which means the mathematical description of the electrochemical process can be simplified. This thesis will focus on transmission thin-layer spectroelectrochemical measurements in the IR region using an optically transparent diamond electrode. IR offers an advantage over other spectroscopies that have been coupled to electrochemistry (e.g., UV/vis), because it provides information about the identity and molecular structure of a reactive species.

1.2 Optically Transparent Electrodes (OTE)

Transmission spectroelectrochemical measurements require an electrode that is transparent to the electromagnetic radiation. An ideal OTE would possess good electrical conductivity and high optical transparency.

A. Minigrid OTE



B. Film-Based OTE

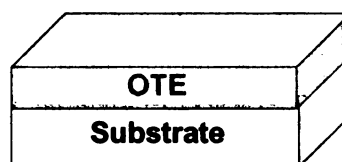


Figure 1-2 Two conventional OTEs for transmission measurements: (A) a metal minigrid and (B) a thin film supported on an optically transparent substrate.

Electrode architecture that would work for such a measurement is a porous electrode. One example is a minigrid electrode (e.g., Au, Ni, Ag or Cu),⁹⁻¹¹ which is simply a metal mesh (Figure 1-2 A), and porous reticulated vitreous carbon.^{12, 13} Light is transmitted through the electrode openings allowing one to probe changes in electronic properties or structural features of a molecule brought about by a change in redox state.

The other design is a thin film (Figure 1-2 B) supported on an optically transparent substrate. Depending on the spectral region of interest, conductive thin films,

such as metals^{14, 15}, carbon materials¹⁶⁻¹⁸ and metal oxides,¹⁹⁻²¹ are used. The most common OTE material is indium-doped tin oxide (ITO), which is deposited as a thin film on a transparent substrate, such as glass (visible), quartz (UV-visible), germanium or silicon (infrared). Optically transparency results because of the thinness of the conducting film. Usually, a compromise between the electrical conductivity and the transparency has to be made as these two parameters are inversely related to one another. A transparent substrate can be used to increase the mechanical stability of the thin OTE.

For IR transmission spectroelectrochemical measurements, a gold or platinum minigrad is the most commonly used electrode material. They are easily fabricated and transparent over the whole electromagnetic spectrum. Modified gold minigrad electrodes are used more often than the bare gold minigrad. The disadvantages of this electrode type are the narrow potential window, the large background charging current and the effort needed to modify the surface and the selection of mediators. Due to their geometry, they are not suited to optical probing of surface localized processes such as adsorption and chemical modification. Also, their fragility limits the lifetime of the cell constructed using them. A more stable OTE material is needed in order to enable more widespread application of this informative technique.

1.3 Development of Optically Transparent Boron-Doped Diamond Electrode

1.3.1 Boron-Doped Diamond Electrode

The use of electrically conductive diamond as an electrode material is a field of research that had its beginning back in the early 1990s.²²⁻²⁴ Diamond is the hardest natural material, consisting of a crystal lattice of tetrahedrally-arranged sp^3 -bonded carbon atoms. This arrangement leads to six-membered rings in a chair conformation, as shown in Figure 1-3.²⁵

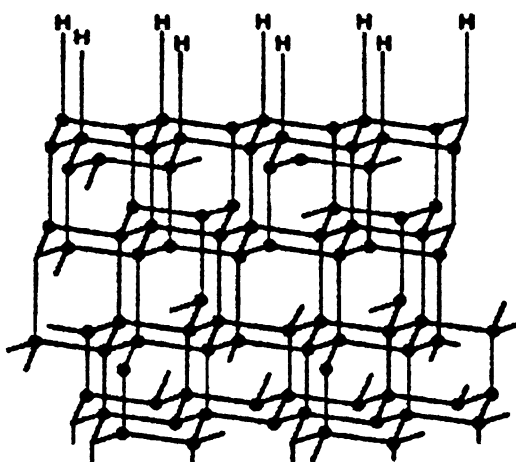


Figure 1-3 Schematic of bonding arrangement of sp^3 -bonded diamond. (adapted with permission from reference 25)

It can be produced synthetically by two methods: (1) high-pressure-high-temperature (HPHT) growth ($>1400\text{ }^\circ\text{C}$, $>50,000\text{ bar}$) in the presence of a catalyst, and (2) low pressure, low temperature ($<1000\text{ }^\circ\text{C}$, $0.01\text{-}1\text{ bar}$) chemical vapor deposition (CVD) from a carbon-containing source gas mixture.²⁶ CVD diamond is usually polycrystalline with randomly-oriented crystallites and grain boundaries between the crystallites. These grain

boundaries consist of a mixture of sp^2 - and sp^3 - bonded carbon. Diamond is naturally an insulating material, so in order for it to be electrically conducting, it must be doped. Boron dopant atoms substitute for carbon atoms in the growing crystal lattice, which produces *p-type* semiconductivity with an acceptor level 0.37 eV above the valence band.²⁷ Resistivities as low as 0.01 Ω -cm have been reported for degenerately boron-doped films, making them useful as electrochemical electrodes.^{28, 29} The surface carbon atoms are stabilized by strong covalent bonds with hydrogen for films deposited from hydrogen-rich source gas mixtures, as illustrated in Figure 1-3.

The application of boron-doped diamond thin-film electrodes in electroanalysis has received much attention in recent years.^{27, 28, 30, 31} Much of the work so far has involved the characterization of the physical and electrochemical properties of boron-doped diamond and its electrochemical response toward a variety of aqueous and nonaqueous redox systems.³²⁻³⁶ From the results, it can be concluded that *high-quality* diamond, which means minimal nondiamond carbon impurity content, low secondary nucleation density, and hydrogen surface termination, offers significant advantages over other carbon and metal electrodes in terms of a wide potential window, lower and more stable background current, fouling resistance, lower limits of detection, and better robustness.^{27, 30, 37, 38}

1.3.2 Optically Transparent Boron-Doped Diamond Electrode

Another unique property of diamond is its optical transparency. Diamond (undoped) has one of the widest optical windows of any material extending from the band gap absorption edge (~ 225 nm) deep into the far infrared (~ 30 cm^{-1}). Factors that

influence the optical throughput of diamond include the defect density, dopant type and doping level, film thickness and grain size (roughness). Adding boron dopant to improve the electrical conductivity will reduce the optical throughput in isolated regions of the spectrum. It is therefore essential to establish a balance between the electrical and optical properties of boron-doped diamond in order to make the material a useful OTE. By adjusting the CVD growth conditions, it is possible to manipulate and optimize this balance.

The versatility of boron-doped diamond, both as an electrode and an optically transparent material, makes it an obvious choice for spectroelectrochemical measurements.³⁹ In general, the diamond offers several advantages over other commonly used OTEs, including (1) a wide optical window extending from near UV into far-IR regions of the electromagnetic spectrum, (2) a wide working potential window and low background current, (3) stability during both cathodic and anodic polarization even at high current density and potential, (4) reproducibility of the electrical, optical and electrochemical properties from batch-to-batch, and (5) resistance to fouling because of a nonpolar, hydrogen-terminated surface.³⁹

Our group has been developing optically transparent diamond electrodes for use in the spectroelectrochemical measurements for some time now.³⁹⁻⁴³ Both free-standing diamond disks and diamond thin film deposited on quartz or undoped Si have been prepared, characterized and utilized in transmission spectroelectrochemical measurements. Zak et al. characterized a free-standing diamond disk in a thin-layer spectroelectrochemical cell for UV-vis transmission measurements of $\text{Fe}(\text{CN})_6^{-3/4}$ and methyl viologen.⁴⁰ Haymond et al. applied the free-standing diamond disk to the study of

ferrocene in acetonitrile.⁴² Their works demonstrated that the boron-doped diamond is a practical OTE material for reproducible spectroelectrochemical measurements both in aqueous and nonaqueous media. However, due to the large thickness (380 μm), the transparency was limited. In general, the low transparency, the long deposition time and laborious mechanical polishing needed to smooth the surface are limitations of this OTE architecture. Stotter et al. reported on the preparation and characterization of a thin film of optically transparent boron-doped diamond deposited on quartz for UV-vis spectroelectrochemical measurements.⁴¹ Absorption spectra of chlorpromazine and $\text{Fe}(\text{CN})_6^{-3/4}$ were recorded at different potentials, and the changes were correlated with alterations in redox state of the molecules. Stotter et al. also compared the electrical, optical, and electrochemical properties of two optically transparent electrodes: diamond and indium tin oxide (ITO).³⁹ Boron-doped diamond has also been deposited on undoped silicon and been used in preliminary mid-IR spectroelectrochemical studies of cytochrome *c*. Such measurements allow one to probe the amino acid side chain and peptide backbone vibrations as a function of the redox state of the protein.⁴³

Compared to diamond deposited on quartz for use in the UV-vis region, work is still needed to optimize the substrate preparation and deposition conditions for preparing uniform, electrically conductive and IR transparent diamond thin film. For use in the mid-IR down to about 700 cm^{-1} , undoped Si is a suitable substrate. Martin and Morrison produced the only other report on IR spectroelectrochemical measurements with diamond. They reported on the internal reflection IR spectroelectrochemical measurement of carbon-oxygen functional groups formed on the diamond surface during anodic polarization in acid.⁴⁴

The long-term goal of this project is to fabricate, characterize and apply transparent diamond electrodes for spectroelectrochemical measurements in the mid- and far- IR. We desire to use this new OTE to elucidate structural changes in redox systems as a function of the redox state. This thesis will describe: (1) the optimum substrate preparation and deposition conditions required for preparing uniform, electrically conductive and IR transparent thin films of diamond on undoped Si, (2) the characterization of the physical, electrical, optical and electrochemical properties of the diamond/Si OTE, (3) the testing of the performance of a new thin-layer spectroelectrochemical cell design that can house the diamond OTE, and (4) the functioning of the OTE in IR transmission spectroelectrochemical measurements.

1.4 Outline of Thesis

This thesis describes the development and characterization of optically transparent boron-doped diamond deposited on undoped silicon as well as its application in IR transmission spectroelectrochemical measurements. Chapter 2 details the experimental parameters and procedures used in the work including the methods, instrumentation, and materials. The fabrication as well as the optical, electrochemical and physical characterization of the diamond/Si OTE are discussed in Chapter 3. The evaluation of these properties is critical for application of the diamond/Si OTE in spectroelectrochemical measurements. In Chapter 4, the performance of the diamond/Si OTE in the IR transmission spectroelectrochemistry is described in which a specially designed thin layer cell was used for the first time. Finally, Chapter 5 summarizes the key findings from the work and provides some future perspectives.

1.5 References

- (1) Heineman, W. R.; Hawkridge, F. M.; Blount, H. N. In *Electroanalytical Chemistry*; Bard, A. J., Ed.; Marcel Dekker: New York, 1984; Vol. 13, pp 1-113.
- (2) Heineman, W. R. *Journal of Chemical Education* **1983**, *60*, 305-308.
- (3) Kuwana, T.; Darlington, K. R.; Leedy, D. W. *Anal. Chem.* **1964**, *36*, 2023-2025.
- (4) McKinley, A. B.; Kenny, C. F.; Martin, M. S.; Ramos, E. A.; Gannon, A. T.; Johnson, T. V.; Dorman, S. C. *Spectroscopy Letters* **2004**, *37*, 275-287.
- (5) Orcajo, O.; Ventosa, E.; Martinez, A.; Colina, A.; Heras, A.; Ruiz, V.; Lopez-Palacios, J. *Journal of Electroanalytical Chemistry* **2006**, *596*, 95-100.
- (6) Palacios, R. E.; Fan, F.-R. F.; Bard, A. J.; Barbara, P. F. *J. Am. Chem. Soc.* **2006**, *128*, 9028-9029.
- (7) Bard, A. J.; Faulkner, L. R. In *Electrochemical Methods: Fundamentals and Applications*, 2 ed.; John Wiley & Sons: New York, 2001, pp 680-735.
- (8) Heineman, W. R. *Anal. Chem.* **1978**, *50*, 390A-402A.
- (9) Murray, R. W.; Heineman, W. R.; O'Dom, G. W. *Anal. Chem.* **1967**, *39*, 1666-1668.
- (10) Petek, M.; Neal, T. E.; Murray, R. W. *Anal. Chem.* **1971**, *43*, 1069-1074.
- (11) Blaedel, W. J.; Boyer, S. L. *Anal. Chem.* **1973**, *45*, 258-263.
- (12) Norvell, V. E.; Mamantov, G. *Anal. Chem.* **1977**, *49*, 1470-1472.
- (13) Sorrels, J. W.; Dewald, H. D. *Anal. Chem.* **1990**, *62*, 1640-1643.
- (14) Yildiz, A.; Kissinger, P. T.; Reilley, C. N. *Anal. Chem.* **1968**, *40*, 1018-1024.
- (15) Benken, W. v.; Kuwana, T. *Anal. Chem.* **1970**, *42*, 1114-1116.
- (16) DeAngelis, T. P.; Hurst, R. W.; Yacynych, A. M.; Mark, H. B., Jr.; William R, H.; Mattson, J. S. *Anal. Chem.* **1977**, *49*, 1395-1398.
- (17) Zak, J.; Porter, M. D.; Kuwana, T. *Anal. Chem.* **1983**, *55*, 2219-2222.
- (18) Anjo, D. M.; Brown, S.; Wang, L. *Anal. Chem.* **1993**, *65*, 317-319.
- (19) Armstrong, N. R.; Lin, A. W. C.; Fujihira, M.; Kuwana, T. *Anal. Chem.* **1976**, *48*, 741-750.
- (20) Ginley, D. S.; Bright, C. *MRS Bull.* **2000**, *25*, 15-18.

- (21) Donley, C.; Dunphy, D.; Paine, D.; Carter, C.; Nebesny, K.; Lee, P.; Alloway, D.; Armstrong, N. R. *Langmuir* **2002**, *18*, 450-457.
- (22) Bachmann, P. K.; Leers, D.; Lydtin, H. *Diamond and Related Materials* **1991**, *1*, 1-12.
- (23) Liu, H.; Dandy, D. S. *Diamond and Related Materials* **1995**, *4*, 1173-1188.
- (24) Ashfold, M. N. R.; May, P. W.; Rego, C. A.; Everitt, N. M. *Chemical Society Reviews* **1994**, 21-30.
- (25) Fischer, A. Ph. D. dissertation, Michigan State University, East Lansing, MI, 2005.
- (26) Pankove, J. I.; Qiu, C. In *Synthetic Diamond: Emerging CVD Science and Technology*; Spear, K. E., Dismukes, J. P., Eds.; John Wiley & Sons: New York, 1994.
- (27) Swain, G. M.; Anderson, A. B.; Angus, J. C. *MRS Bull.* **1998**, *23*, 56-59.
- (28) Xu, J.; Swain, G. M. *Anal. Chem.* **1998**, *70*, 1502-1510.
- (29) Granger, M. C.; Witek, M.; Xu, J.; Wang, J.; Hupert, M.; Hanks, A.; Koppang, M. D.; Butler, J. E.; Lucazeau, G.; Mermoux, M.; Strojek, J. W.; Swain, G. M. *Anal. Chem.* **2000**, *72*, 3793-3804.
- (30) Xu, J.; Granger, M. C.; Chen, Q.; Strojek, J. W.; Lister, T. E.; Swain, G. M. *Anal. Chem.* **1997**, *69*, 591A-597A.
- (31) Rao, T. N.; Yagi, I.; Miwa, T.; Tryk, D. A.; Fujishima, A. *Anal. Chem.* **1999**, *71*, 2506-2511.
- (32) Pleskov, Y. V.; Sakharova, A. Y.; Krotova, M. D.; Builov, L. L.; Spitsyn, B. V. *J. Electroanal. Chem. and Interfac. Electrochem.* **1987**, *228*, 19-27.
- (33) Mermoux, M.; Roy, F.; Marcus, B.; Abello, L.; Lucazeau, G. *Diamond and Related Materials* **1992**, *1*, 519-524.
- (34) Strojek, J. W.; Granger, M. C.; Swain, G. M.; Dallas, T.; Holtz, M. W. *Anal. Chem.* **1996**, *68*, 2031-2037.
- (35) Holt, K. B.; Bard, A. J.; Show, Y.; Swain, G. M. *J. Phys. Chem. B* **2004**, *108*, 15117-15127.
- (36) Mora, A. E.; Steeds, J. W.; Butler, J. E. *Diamond and Related Materials* **2002**, *11*, 697-702.
- (37) Rao, T. N.; Loo, B. H.; Sarada, B. V.; Terashima, C.; Fujishima, A. *Anal. Chem.* **2002**, *74*, 1578-1583.

- (38) Fujishima, A.; Rao, T. N.; Try, D. A. *Proc.-Electrochem. Soc.* **2000**, 99-32, 383-388.
- (39) Stotter, J.; Show, Y.; Wang, S.; Swain, G. *Chem. of Mater.* **2005**, 17, 4880-4888.
- (40) Zak, J. K.; Butler, J. E.; Swain, G. M. *Anal. Chem.* **2001**, 73, 908-914.
- (41) Stotter, J.; Zak, J.; Behler, Z.; Show, Y.; Swain, G. M. *Anal. Chem.* **2002**, 74, 5924-5930.
- (42) Haymond, S.; Zak, J. K.; Show, Y.; Butler, J. E.; Babcock, G. T.; Swain, G. M. *Anal. Chim. Acta* **2003**, 500, 137-144.
- (43) Stotter, J.; Haymond, S.; Zak, J. K.; Show, Y.; Cvackova, Z.; Swain, G. M. *Interface* **2003**, 12, 33-38.
- (44) Martin, H. B.; Morrison, P. W. *Electrochem. and Solid-State Lett.* **2001**, 4, E17-E20.

CHAPTER 2

Experimental Methods

2.1 Diamond Thin Film Deposition

The diamond thin-film electrode was deposited by microwave-assisted chemical vapor deposition (1.5 kW, 2.54 GHz, Astex, Inc., Lowell, MA).¹ A diagram of a typical reactor is shown in Figure 2-1.

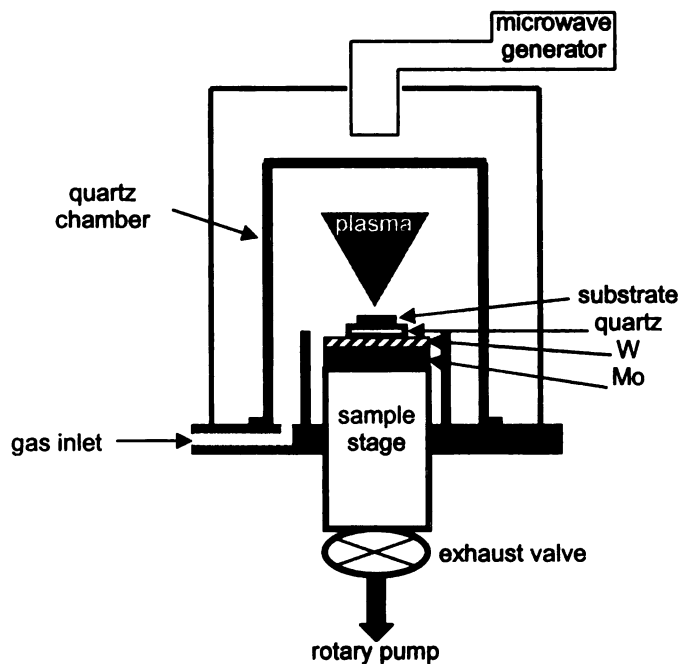


Figure 2-1 A schematic of a microwave plasma-assisted CVD reactor used to grow boron-doped diamond thin-film electrodes.

Ultrahigh purity (99.999%) methane, hydrogen, and diborane were used as the source gases. They entered the chamber at controlled rates regulated by mass flow

controllers. The microwave plasma was then ignited inside a quartz cavity with the flowing source gases. The pressure of the chamber was regulated using a throttle exhaust valve in series with a rotary pump.

Before growth, the nominally undoped Si (100) substrate ($>100 \text{ } \Omega\text{-cm}$, $500 \text{ } \mu\text{m}$ in thickness, Virginia Semiconductor, Inc., Fredericksburg, VA) was mechanically scratched for 5 min on a felt pad using a 100 nm diameter diamond powder (Diamond Innovations, Worthington, OH) suspended in ultrapure water. The substrate was then sonicated for 5 min each in ultrapure water, 2-propanol, acetone, 2-propanol, and ultrapure water to remove polishing debris from the surface, especially from the scratches or striations. The substrate was then dried and examined under an Olympus BX60M optical microscope (Olympus America, Inc.) for cleanliness. Embedded diamond powder particles as well as the scratching defects serve as the initial nucleation sites for diamond growth.

The diamond film was then deposited using a $\text{CH}_4/\text{H}_2/\text{B}_2\text{H}_6$ source gas mixture consisting of 0.5% CH_4/H_2 with 2 ppm B_2H_6 added for boron doping, a total gas flow of 200 sccm, a power of 1000 W, a system pressure of 45 torr, a substrate temperature of $\sim 750 \text{ } ^\circ\text{C}$ (estimated via an optical pyrometer), and a growth time of 4 h. At the end of the deposition period, the CH_4 and B_2H_6 gas flows were stopped and the film remained exposed to an H_2 plasma for an additional 10 min at 1000 W and 45 Torr. The plasma power and pressure were then slowly reduced over a 5-min period to cool the samples to a temperature below $300 \text{ } ^\circ\text{C}$ in the presence of atomic hydrogen. The plasma power was then turned off, and the film was cooled to room temperature under a flow of H_2 . This post-growth annealing procedure in atomic hydrogen is needed to remove adventitious

nondiamond sp^2 carbon impurity, to minimize dangling bonds, and to ensure full hydrogen termination.

2.2 Material Characterization

A number of analytical methods were used to characterize the diamond/Si OTE properties, including scanning electron microscopy, Raman spectrometry, four-point probe electrical resistance measurements, IR spectroscopy, and electrochemical measurements.

2.2.1 Scanning Electron Microscopy (SEM)

The film morphology was probed by SEM using a JSM-6400 microscope (JEOL, Ltd., Tokyo, Japan, Center for Advanced Microscopy at Michigan State University) with a 20 kV accelerating voltage and a working distance of 15 mm. Due to the low conductivity of the undoped silicon substrate, the diamond film edges were connected to the aluminum stub using conductive carbon tape. This reduced surface charging effects and improved the image quality. The tape also served to affix the electrode to the aluminum stub.

2.2.2 Raman Spectroscopy

Raman spectroscopy was used to evaluate the microstructure of the diamond/Si OTE. A Chromex Raman 2000 spectrograph (Chromex, Inc., Albuquerque, NM) was employed that consisted of a diode-pumped, frequency-doubled CW Nd:YAG laser (500 mW at 532 nm, Coherent), a Chromex 500is spectrometer (f/4, 600 grooves/mm

holographic grating, 50 μm slit width) and a thermoelectrically-cooled 1024 \times 256 element charge-coupled device (CCD) detector was used to illuminate the sample surface. All spectra were recorded at room temperature with an incident power density of ca. 500 kW/cm^2 (100 mW at the sample and 5 μm diameter spot size) and a 10 s integration time. The spectrograph was first calibrated using the spectrum of acetaminophen (tylenol) and double checked with a high-pressure, high-temperature (HPHT), single crystal diamond sample (first-order phonon position = 1332 cm^{-1}). A white-light spectrum was collected using the same conditions and this served as the background.

2.2.3 X-Ray Diffraction Spectroscopy (XRD)

The crystallinity of diamond thin film was investigated by powder XRD. Spectra were obtained by scanning 2θ from 20° to 100° using a Rigaku Rotaflex RTP300 RC diffractometer equipped with a rotating anode and a Cu $K\alpha$ radiation source (1.540 \AA).

2.2.4 Four-Point Probe Measurements

The electrical resistivity of the diamond/Si OTE was measured using an in-line arrangement, four-point tungsten-tip probe connected to an HP 3748A multimeter (Hewlett-Packard, Palo Alto, CA). The meter was operated in the four-wire resistance measurement mode with a probe spacing of 0.1 cm. A constant current was applied between the outer two probes and the voltage drop between the inner two probes was measured. The resistance was determined from I-V data and converted to a resistivity value according to equation,²

$$\rho (\Omega\cdot\text{cm}) = 4.532 l (\text{cm}) R (\Omega)$$

where l is the film thickness in centimeters. Multiple measurements were made at different locations on each electrode.^{3,4}

2.2.5 Optical Transmission Measurements

The diamond/Si OTE was rinsed with clean isopropanol (IPA) and dried with nitrogen prior to making a transmission measurement. The alcohol was distilled and stored over activated carbon prior to use.⁵ The electrode was positioned in the light path using a small piece of double-sided adhesive tape. The sample was mounted vertically for the IR transmission measurements with the diamond surface facing the incident light beam. All IR spectra were recorded using a ATI Mattson Research Series 1 spectrometer with an liquid nitrogen-cooled MCT detector. Typically, spectra were acquired using an average of 100 scans at a 4 cm^{-1} resolution.

2.2.6 Electrochemical Characterization

Cyclic voltammetry was the main method used to characterize the electrochemical properties of the OTEs.^{6,7} All the electrochemical measurements were performed at room temperature with a computer-controlled potentiostat (Model 650A, CH Instruments, Inc., Austin, TX) in a standard three-electrode configuration, as shown in Figure 2-2.⁸

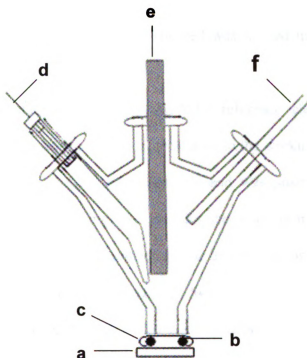


Figure 2-2 Design of the single-compartment, three-electrode electrochemical cell with (a) the diamond film working electrode, (b) O-ring seal, (c) nickel foil and rubber spacer, (d) reference electrode inside a glass capillary tube with a cracked tip, (e) carbon rod counter electrode, and (f) input for nitrogen purge gas. (adapted with permission from reference 8)

The working electrode was clamped to the bottom opening of a single-compartment, glass electrochemical cell. A Viton[®] O-ring (i.d. 0.5 cm), placed between the cell opening and the electrode surface, defined the electrode area exposed to the solution (0.2 cm^2). Contact was made to the working electrode by pressing a neoprene rubber spacer and a piece of nickel foil against the entire film surface outside the O-ring. The O-ring was sonicated for 10 min in ultrapure water, rinsed with distilled IPA, and dried with a stream of N_2 before use. The electrode was then soaked in clean IPA for 20 min before any measurements.^{5,9} After rinsing thoroughly with distilled water, the cell was filled with the electrolyte solution of interest. Nitrogen was bubbled through the

solution for 15 min to displace dissolved oxygen and the solution was blanketed by the gas during the entirety of a measurement. The cell was housed in a Faraday cage for electrical shielding.

In aqueous media, a home-made Ag/AgCl reference electrode (4 M NaCl saturated with AgCl) was positioned in close proximity to the working electrode. A large-area carbon rod served as the auxiliary electrode and was positioned normal to the working electrode. A Viton[®] O-ring was used for the aqueous measurements. No iR compensation was applied to the voltammetric data. In nonaqueous media (ferrocene), a ChemRaz[®] (Ace Glass) O-ring was employed. A Ag wire, encased in Teflon[®], served as the quasi-reference electrode, and a Pt foil was used as the auxiliary electrode. A low analyte concentration (0.1 mM) and iR compensation were used in the voltammetric measurements of ferrocene in an effort to minimize ohmic effects in the wave shape. Digital compensation of the uncompensated solution resistance was accomplished via a positive-feedback method.

2.3 Spectroelectrochemical Measurements

FTIR spectra were measured using a Bruker Equinox 55 spectrometer with a MCT detector. All spectra presented are an average of 128 scans recorded at 4 cm⁻¹ resolution. The electrode potential was controlled with an Omni-90 analog potentiostat (Cypress Systems, Inc.) in the constant potential mode.

2.3.1 Thin-Layer Spectroelectrochemical Cell

A new, custom-built transmission thin-layer cell, as shown in Figure 2-3,¹⁰ was used for the IR spectroelectrochemical measurements. A film spacer of desired thickness ($7.5\ \mu\text{m}$ for $\text{Fe}(\text{CN})_6^{-3/4}$ and $75\ \mu\text{m}$ for ferrocene in this work) compressed between the working OTE and the IR window (CaF_2 , 9 mm dia. x 5 mm and Si, 9 mm dia. x $500\ \mu\text{m}$ (used together with spacer)) determined electrochemical cavity. The cell was equipped with an integral, miniature Ag/AgCl reference electrode for aqueous solution and a platinum wire quasi-reference electrode (QRE) for nonaqueous solution. A platinum wire ring outside the sealed cavity was used to establish electric contact with the working electrode. Another Pt wire, encircling the rear of the IR window several times, formed the auxiliary electrode. Analyte solution was injected into the cell cavity with a syringe.

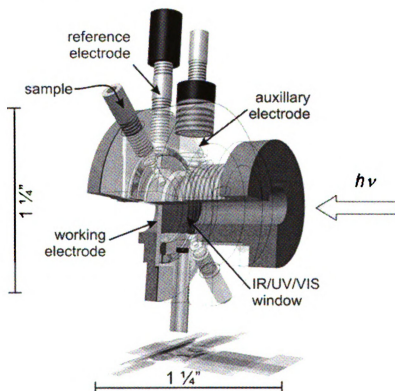


Figure 2-3 Diagram of the IR transmission thin-layer spectroelectrochemical cell.

2.3.2 Potential Step Method

Spectroelectrochemical measurements were made by stepping the potential from a value where the redox system was stable (e.g. reduced form) to values where the redox reaction (e.g., oxidation) occurred. An absorbance spectrum was collected at each potential after a equilibration period (e.g. 1 min) at each potential, as depicted in Figure 2-4.

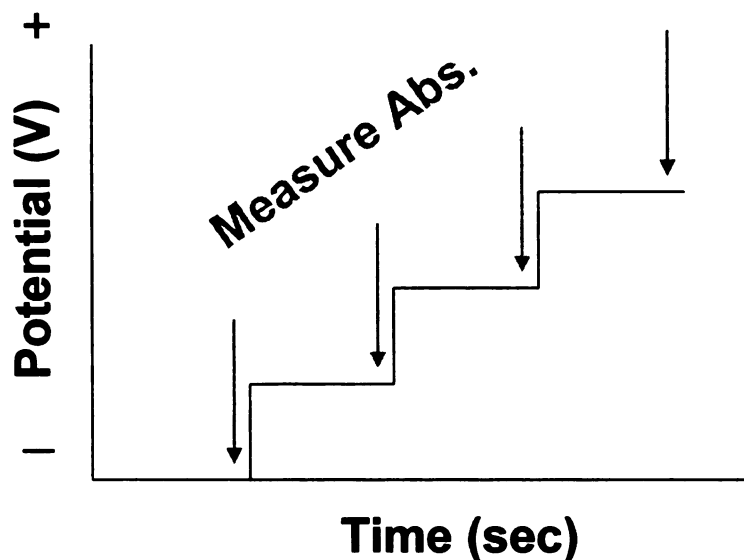


Figure 2-4 Potential-time profile for the recording of spectroelectrochemical measurements. An absorbance spectrum was recorded at each potential as indicated by the arrows.

Absorbance difference spectra were then generated by subtracting the spectrum for the unreacted redox system from the spectrum obtained at each potential of the redox reaction. Small absorbance changes that occur during the transition between redox states are not always obvious. They are identifiable when a difference absorbance spectrum is generated. Figure 2-5 shows an idealized difference spectrum with negative going bands

being characteristic of the initial state A, and positive going bands reflective of product state B.¹¹

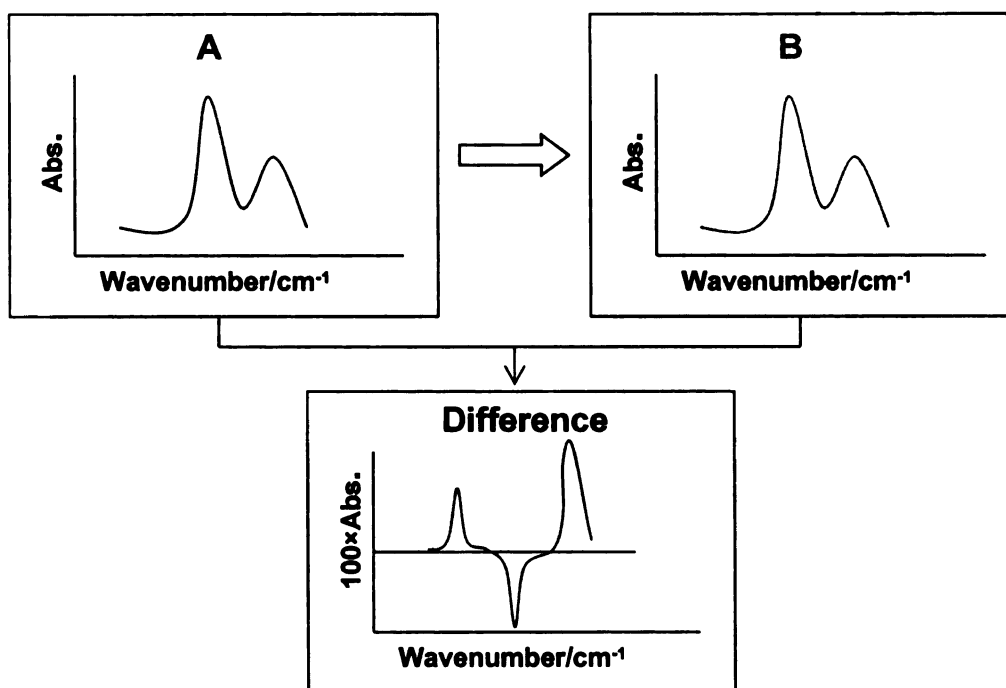


Figure 2-5 Principle of absorbance difference spectroscopy.

2.3.3 Temperature Control

For the IR spectroelectrochemical measurements, the spectroelectrochemical cell was loaded with the sample and mounted onto a support inside a sealed, thermostated chamber. The temperature was controlled by Lakeshore model 340 temperature controller using 200 Ohm thermistors (YSI Inc., Dayton, OH) to suppress the thermal contributions. A constant stream of dry nitrogen gas was used to control the temperature and to purge water vapor/CO₂ from chamber. The gas was first cooled by passage through a heat exchange in a solid CO₂ (dry ice)/ethanol bath followed by heating with 50 Ohm

resistance wire inside a glass transfer line. A thermistor suspended in the vicinity of, but not attached to, the thin-layer spectroelectrochemical cell was used for temperature measurement and control. Separate sensors one at the gas inlet and another imbedded in the body of the cell were used to optimize the control parameters for temperature stability (≤ 0.02 °C) and response ($\tau \approx 20$ min). This setup allowed for quick purging of the sample compartment and precise temperature control. The temperature was regulated at 19 ± 0.01 °C in this work.

2.4 Chemicals

All chemicals were reagent grade quality, or better, and were used without additional purification. Solutions of 0.1 mM potassium ferrocyanide (Aldrich), hexaammineruthenium (III) chloride (Aldrich), methyl viologen (Aldrich), potassium hexachloroiridate (IV) (Aldrich) in 1 M potassium chloride (CCI) were prepared fresh daily with ultrapure water (~ 18 M Ω -cm) from a commercial water purification system (Barnstead E-pure). Ferrocene (Aldrich) was dissolved in 0.1 M tetrabutylammonium tetrafluoroborate (TBABF₄) (99%, Aldrich) plus acetonitrile (ACN). The ACN was purified by distillation followed by storage over 3 Å molecular sieves. The molecular sieves were activated by heating at 300 °C for 15 h followed by cooling in a desiccator. After storage over the activated sieves (5-10% w/v) for several days, ACN was transferred to a clean amber bottle and allowed to stand over a second batch of molecular sieves.¹² All glassware was cleaned in a three-step manner: KOH-ethanol bath,alconox/ultrapure water solution, and ultrapure water rinse.

2.5 References

- (1) Swain, G. M. In *Electroanalytical Chemistry*; Bard, A. J., Rubinstein, I., Eds.; Marcel Dekker, 2004; Vol. 22, pp 182-277.
- (2) Schroder, D. K. *Semiconductor Material and Device Characterization*, 2 ed.; John Wiley & Sons: New York, 1990.
- (3) Stotter, J.; Zak, J.; Behler, Z.; Show, Y.; Swain, G. M. *Anal. Chem.* **2002**, *74*, 5924-5930.
- (4) Stotter, J.; Show, Y.; Wang, S.; Swain, G. *Chem. of Mater.* **2005**, *17*, 4880-4888.
- (5) Ranganathan, S.; Kuo, T.-C.; McCreery, R. L. *Anal. Chem.* **1999**, *71*, 3574-3580.
- (6) Nicholson, R. S. *Anal. Chem.* **1965**, *37*, 1351-1355.
- (7) Bard, A. J.; Faulkner, L. R. In *Electrochemical Methods: Fundamentals and Applications*, 2 ed.; John Wiley & Sons: New York, 2001.
- (8) Granger, M. C.; Witek, M.; Xu, J.; Wang, J.; Hupert, M.; Hanks, A.; Koppang, M. D.; Butler, J. E.; Lucazeau, G.; Mermoux, M.; Strojek, J. W.; Swain, G. M. *Anal. Chem.* **2000**, *72*, 3793-3804.
- (9) Show, Y.; Witek, M. A.; Sonthalia, P.; Swain, G. M. *Chem. Mater.* **2003**, *15*, 879-888.
- (10) Dai, Y.; Proshlyakov, D. A.; Swain, G. M. In *58th Pittsburgh Conference on Analytical Chemistry and Applied Spectroscopy*: Chicago, IL, 2007.
- (11) Zscherp, C.; Barth, A. *Biochem.* **2001**, *40*, 1875-1883.
- (12) Fry, A. J. In *Laboratory Techniques in Electroanalytical Chemistry : Second Edition, Revised and Expanded*; Kissinger, P. T., Heineman, W. R., Eds.; Marcel Dekker: New York, 1996.

CHAPTER 3

Optical, Electrical, Physical and Electrochemical Properties of the Boron-Doped Diamond Electrodes

3.1 Introduction

Optically transparent boron-doped diamond electrodes were prepared by microwave plasma-assisted chemical vapor deposition (CVD), as described in Chapter 2. An ideal OTE would possess these optical and electrochemical properties: a wide optical window, a low and stable background current over a wide working potential window, good activity towards redox systems without the need for pretreatment, chemical stability and fouling resistance.

Diamond has the widest optical window of any known material, ranging from the fundamental absorption edge at 0.22 μm to the far-IR.¹ We are specifically interested in the optical transparency of diamond OTE in the infrared region of the electromagnetic spectrum. In the IR region, the optical transparency of diamond OTE is affected by several factors that are listed below.¹

First, absorption by chemical impurities and defects, such as adventitiously incorporated nitrogen and nondiamond sp^2 bonded carbon, result in the throughput loss due to the loss of the lattice symmetry. For example, substitutional nitrogen leads to a peak at 1100 cm^{-1} ,^{2,3} and the CH stretch for sp^2 -bonded carbon has characteristic peaks between 3000 cm^{-1} and 3200 cm^{-1} .^{4,5}

Second, absorption by the boron acceptor band lowers the optical throughput. Absorbance peaks at 2460, 2800 and 2930 cm^{-1} are characteristic of substitutionally inserted boron and these peaks are associated with transitions from the ground state to the first, second and third excited states, respectively ^{2,3,6-8}. These absorption bands broaden considerably at high boron concentrations ($>10^{19} \text{ B cm}^{-3}$) ².

Third, scattering losses reduce the optical transparency. Scattering occurs because of the surface roughness of the polycrystalline films or scattering centers in the films. ^{1,9}

Fourth, reflectance losses reduce the light throughput due to the high refractive index of diamond, which is ca. 2.4 in the IR region (500 to 5000 cm^{-1}). ¹ According to the Fresnel equation ($\theta = 0^\circ$), a reflectance loss of 17% is calculated for the diamond/air interface, and a 3% loss is calculated for the diamond/silicon interface. The calculated 17% loss at the diamond/air interface is in good agreement with the 80% transparency of a free-standing diamond disc. (see Figure 3-1)

Fifth, film thickness, which affects the transparency according to Beer's law relationship between light path and adsorption.

Through optimization of the deposition conditions, one attempts to minimize the incorporated impurities, defects, surface roughness and film thickness. Most importantly, a balance must be reached between the boron-doping level required for the desired electrical conductivity and the maintenance of sufficient optical transparency. ⁹⁻¹¹

The adventitious incorporation of sp^2 -bonded carbon impurity in diamond films can also reduce the light throughput due to the absorption. ^{4,5} This impurity (specifically at the surface) can also affect the electrochemical properties of the electrode by reducing the working potential window and increasing the background current ^{12,13}. Bennett et al.

described how the ratio of CH₄/H₂ in the source gas mixture affects the amount of sp²-bonded nondiamond carbon impurity incorporated into films grown by microwave CVD.¹³ A CH₄/H₂ ratio of 0.5% provided a relatively rapid diamond growth rate with a low level nondiamond carbon incorporation.¹³ In general, the higher the CH₄/H₂ ratio, the greater the level of nondiamond carbon. Controlling the boron doping level is very important for maximizing the optical transparency while maintaining sufficient electrical conductivity. A relatively smooth film can be obtained if a high instantaneous nucleation density exists during the diamond deposition. This can be achieved by substrate pretreatment (mechanically polishing) before growth. The fine scratching of the substrate surface produces a high initial density of nucleation sites, which leads to the growth of a relatively smooth and continuous film in a short period of time. The growth time can be adjusted to control the film thickness. Postgrowth annealing in the presence of atomic hydrogen is also essential for removing any adventitious sp²-bonded nondiamond carbon impurity and hydrogen terminating the surface. The hydrogen-terminated surface has been reported to resist fouling and generally exhibits the most rapid electron-transfer kinetics for redox couples.^{12, 14} Table 3-1 lists the controllable growth parameters and their effect on the electrical and optical properties of diamond.

Table 3-1 Effect of growth parameters on the properties of the diamond/Si OTE.

Growth Parameter	Diamond OTE Property
CH ₄ /H ₂ ratio ¹³	sp ² -bonded nondiamond impurity
Boron doping level	Balance between the electrical conductivity and optical transparency
Mechanical polishing of the substrate	Surface roughness
Growth time	Film thickness
Hydrogen termination	Fouling resistance

This chapter describes the characterization of the optical, electrical, physical and electrochemical properties of boron-doped diamond thin film. Optical transparency in the IR region is the reason for selecting a particular set of growth conditions, as described herein. Four-point probe measurements were performed to determine the electrical resistivity of the film. The film morphology and microstructure of the diamond thin film were characterized by scanning electron microscopy (SEM) and Raman spectroscopy, respectively. X-ray diffraction (XRD) analysis was used to verify the crystallinity of the electrode. The electrochemical properties of the diamond/Si OTE were investigated by cyclic voltammetry using both in aqueous ($\text{Fe}(\text{CN})_6^{-3/-4}$, methyl viologen, $\text{Ru}(\text{NH}_3)_6^{+3/+2}$ and $\text{IrCl}_6^{-2/-3}$, all in 1 M KCl) and nonaqueous (ferrocene in $\text{TBABF}_4/\text{CH}_3\text{CN}$) redox molecules.

3.2 Results and Discussion

3.2.1 Optical Properties of Diamond/Si OTE-IR

Figure 3-1 shows IR transmission spectra for several different types of boron-doped diamond electrodes: (A) a CVD “white” (type IIa) diamond disc, (B) undoped and polished Si substrate, (C) boron-doped diamond thin film deposited on the undoped Si using 2 ppm B_2H_6 and a 4-h growth time, (D) boron-doped diamond thin film deposited on the undoped Si using 5 ppm B_2H_6 and a 4-h growth time, and (E) boron-doped diamond thin film deposited on the undoped Si using 2 ppm B_2H_6 and a 10-h growth time.

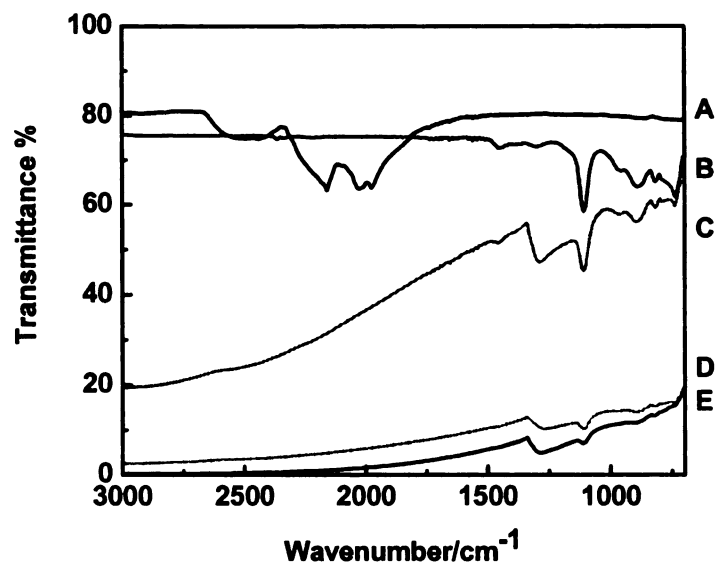


Figure 3-1 IR transmission spectra for different types of boron-doped diamond electrodes. The films are described in the text.

The CVD “white” diamond (Figure 3-1 A) is relatively free of structural defects and chemical impurities and the one-phonon mode is prohibited due to the high degree of lattice symmetry in this type IIa diamond.¹⁵ The absorption bands in the 2666-1333 cm^{-1} region are attributed to the two-phonon absorption and they are intrinsic to all diamond.^{4, 5} The undoped Si substrate (Figure 3-1 B) possesses about 75% transmittance throughout the entire mid-IR with the exception of some weak absorption below 1200 cm^{-1} . The reduced light throughput is attributed to be relatively constant reflectance losses over the entire wavenumber range.⁹ When boron is introduced into the diamond lattice to make it conductive, the transparency decreases, as shown in Figure 3-1 C, D and E. The introduction of boron breaks the lattice symmetry, resulting in the broad absorption centered at 1290 cm^{-1} in the one-phonon vibronic region.^{8, 9, 16} For highly doped films, a broad continuum develops above 2000 cm^{-1} as a consequence of the interaction of the

boron centers, as evident in Figure 3-1 C and D. This continuum leads to a reduction in light throughput to less than 30% for the 4-h film and less than 1% in the 10-h film.

The 4-h film has sufficient conductivity and optical throughput, rendering it useful for spectroelectrochemical measurements. Presently, our moderately boron-doped films transmit approximately 40-60% of the light between 2000 and 700 cm^{-1} . Importantly, the optical transparency of the diamond OTE is stable after extended use in electrochemical measurements, which is a requirement for difference spectroelectrochemical measurements.

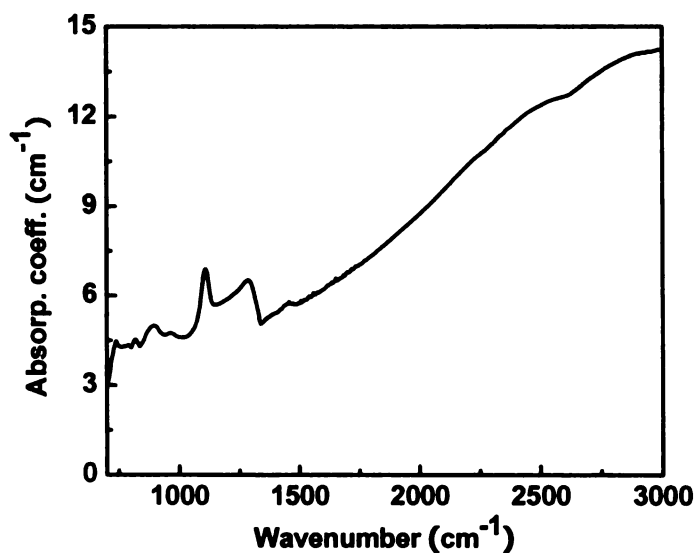


Figure 3-2 IR absorption spectrum of boron-doped diamond/Si OTE deposited for 4 h using 2 ppm B_2H_6 .

Figure 3-2 shows the IR absorption spectrum of boron-doped diamond/Si OTE deposited for 4 h using 2 ppm B_2H_6 . This figure is generated from the Beer's Law using diamond/Si OTE transmission spectrum and total thickness of the diamond + Si substrate

as the pathlength. This format is convenient for comparing materials with different thicknesses.

3.2.2 Electrical Properties of Diamond/Si OTE

The electrical resistivity of the diamond/Si OTE was obtained by a four-point probe measurement. Six measurements were made at different locations on each electrode in order to obtain an average value of the resistivity. Figure 3-3 shows the nominal electrical resistivity for five different diamond OTEs grown the same way. The electrical resistivity of the diamond/Si OTE is comparable from film to film, all in the 0.1 to 0.4 Ω -cm range. Importantly, these films possess the 40-60% transparency below 2000 cm^{-1} , as shown in Figure 3-1.

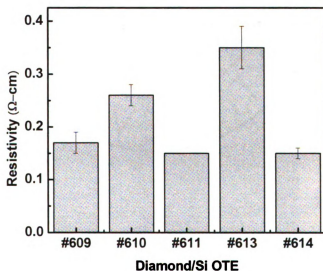


Figure 3-3 Four-point probe electrical resistivity measurements for five different diamond/Si OTEs deposited for 4 h using 2 ppm B_2H_6 .

3.2.3 Physical Properties of Diamond/Si OTE

Representative scanning electron micrographs of the diamond/Si OTE grown for 4 h using 2 ppm B_2H_6 are shown in Figure 3-4. Figure 3-4A clearly reveals the film is well faceted and polycrystalline, and covers the substrate with no visible cracks or voids. The crystallite size ranges from 0.1 to 1 μm . Figure 3-4B shows a side-view image of the diamond layer. The film is dense and homogeneous with a thickness of 1.5 μm .

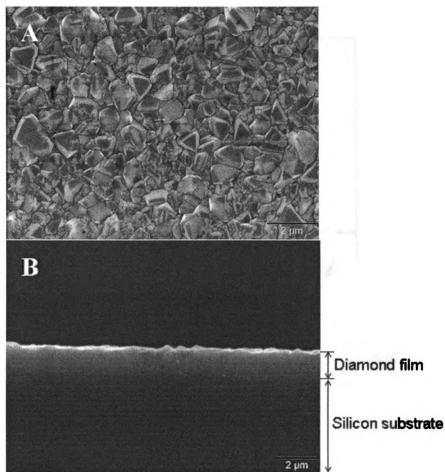


Figure 3-4 Scanning electron micrographs of a diamond/Si OTE: (A) top view and (B) side view. The film was deposited for 4 h using 2 ppm B_2H_6 .

The microstructure of the diamond was probed by Raman spectroscopy. This technique is commonly employed to characterize the microstructure of both sp^2 - and sp^3 -bonded carbon materials.^{17, 18} The first-order diamond phonon line intensity, width and position are all sensitive to the film quality, specifically the crystalline size, boron-doping level, intrinsic stress and defect density.¹⁷⁻¹⁹ A typical Raman spectrum for a film deposited for 4 h using 2 ppm B_2H_6 is presented in Figure 3-5.

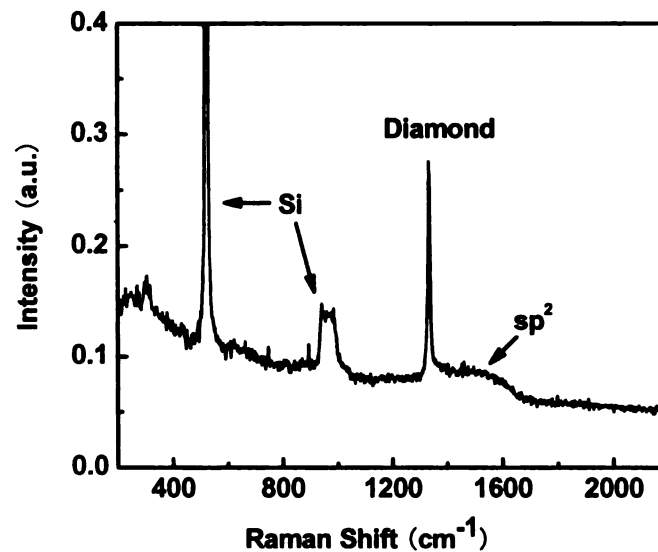


Figure 3-5 Raman spectrum for a diamond/Si OTE deposited for 4 h using 2 ppm B_2H_6 .

The characteristic one-phonon diamond line is present at 1332.7 cm^{-1} with a full width at half maximum (FWHM) of 11 cm^{-1} . This line is asymmetric with an upward shift in the intensity on the high wavenumber side. This asymmetry is attributed to a Fano-type interference, which is caused by quantum interaction between the phonon and a continuum of electronic transitions around the same energy involving the boron

impurity band.²⁰ The FWHM of the diamond phonon peak is, to a first approximation, inversely related to the phonon lifetime and is a measure of the defect density. As stated, the FWHM of the one-phonon line for the diamond film is 11 cm^{-1} ; a value that is comparable with the ca. 8 cm^{-1} typically observed for polycrystalline diamond films grown on Si measured in the same spectrograph.¹² The weak scattering intensity between 1500 and 1600 cm^{-1} is associated with amorphous or sp^2 -bonded nondiamond carbon impurity. With visible excitation, the Raman cross-section for sp^2 -bonded carbon (graphite as the model) is 50 times larger than that for diamond.¹⁸ Therefore, the weak intensity indicates that there is very little sp^2 carbon impurity in the film. The sharp peak at 522 cm^{-1} and the broad peak centered at 960 cm^{-1} are associated with the first-order and second-order phonon modes for the Si substrate.²

Figure 3-6 presents the XRD spectrum for a diamond film grown on undoped Si for 4 h with 2 ppm B_2H_6 . Reflections for the diamond crystalline orientation of (111), (220), and (311) (ASTM 6-0675) are observed and are marked along with the Si (400) (ASTM 27-1402) substrate peak, with the dashed lines, respectively. The broadness of Si (400) peak is likely due to the formation of Si-C at the interface. The spectrum also reflects the high crystalline quality of the diamond as there are no peaks for sp^2 -bonded carbon impurity (d_{002} graphite peak at 26.50 degrees or amorphous carbon peak at 33.96 degrees).²¹ Table 3-2 compares the peak positions and relative intensities with these for a diamond standard from the American Society for Testing and Materials (ASTM). The relative intensity ratio of the (111) and (220) peaks can suggest the change of crystalline orientation of the diamond due to the incorporation of the nondiamond impurity.²² The relative intensity ratio of the two peaks for diamond/Si OTE is 100/24 and is in good

agreement with the expected ratio of 100/25 for cubic diamond, which means relatively low nondiamond impurities in the film.

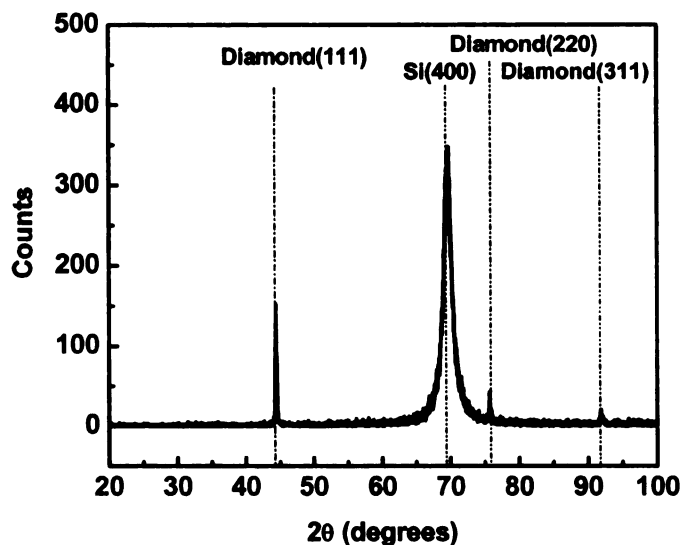


Figure 3-6 Powder X-ray diffraction spectrum of a diamond/Si OTE deposited for 4 h using 2 ppm B₂H₆.

Table 3-2 Comparison between the measured XRD data for a diamond/Si OTE and values from ASTM (6-0675) cubic diamond standard.

Plane	Measured			ASTM (6-0675)		
	2θ (degree)	d-spacing (Å)	Relative Intensity	2θ (degree)	d-spacing (Å)	Relative Intensity
Diamond (111)	44.402	2.0386	100	43.915	2.0600	100
Diamond (220)	75.718	1.2551	24	75.302	1.2610	25
Diamond (311)	91.858	1.0721	13	91.495	1.0754	16

3.2.4 Electrochemical Properties of Diamond OTE

Background cyclic voltammetric *i*-*E* curves are very informative about the boron-doped diamond film quality. The working potential window, magnitude of the

background current, the presence of nondiamond carbon impurity at the surface and the electrical conductivity are all revealed from such measurements. Figure 3-7 shows a background cyclic voltammetric i - E curve in 1 M KCl for a diamond/Si OTE deposited for 4 h using 2 ppm B_2H_6 . The curve is stable with cycling and is largely featureless over the entire potential range, which is typical for films devoid of appreciable quantities of sp^2 -bonded carbon impurity at the surface.¹² The anodic current at 1.3 V is due to the onset of chlorine evolution and the cathodic current at -1.6 V is attributed to hydrogen evolution. The background current for diamond is a factor of 5-10 less than a comparably sized piece of glassy carbon. This leads to improved signal-to-background ratios in electroanalytical measurements with the former.

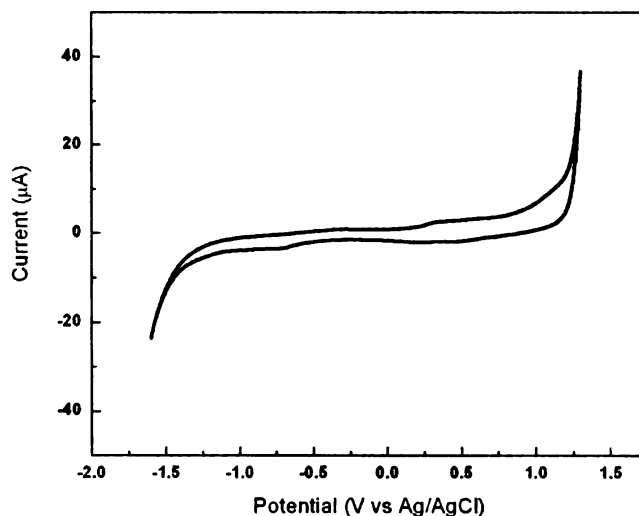


Figure 3-7 Cyclic voltammetric i - E curve in 1 M KCl for a diamond/Si OTE deposited for 4 h using 2 ppm B_2H_6 . Scan rate = 0.1 V/s.

Cyclic voltammetry was used to investigate the electrochemical response of the diamond OTE for different aqueous and nonaqueous redox systems. Representative

cyclic voltammetric i-E curves for 0.1 mM $\text{Fe}(\text{CN})_6^{-3/4}$, methyl viologen, $\text{Ru}(\text{NH}_3)_6^{+3/+2}$ and $\text{IrCl}_6^{-2/-3}$, all in 1 M KCl, and or 0.1 mM ferrocene in 0.1 M $\text{TBABF}_4/\text{CH}_3\text{CN}$, are presented in Figure 3-8 and Figure 3-9. The measurements were made with a diamond/Si OTE grown for 4 h with 2 ppm B_2H_6 . There are two reasons for selecting these redox systems: ¹² (1) the known sensitivity or insensitivity of the heterogeneous electron-transfer rate constant for each to the electronic properties, surface microstructure, and surface chemistry of sp^2 and sp^3 carbon electrodes, and (2) the wide potential range ($\sim +1.1$ to -1.3V vs. Ag/AgCl), the E° values for the redox systems span. $\text{Fe}(\text{CN})_6^{-3/4}$ is a surface-sensitive redox system that undergoes electron transfer through a more inner-sphere electron-transfer pathway. ^{14, 23} The electrode reaction kinetics for this couple are highly sensitive to the diamond surface termination but relatively insensitive to nondiamond sp^2 carbon impurity. ^{14, 24} For methyl viologen, $\text{Ru}(\text{NH}_3)_6^{+3/+2}$ and $\text{IrCl}_6^{-2/-3}$, outer-sphere redox systems, the electrode kinetics are relatively insensitive to the surface microstructure, surface oxides, nondiamond carbon impurity and other defects. ¹⁴ The kinetics are mainly influenced by density of electronic states of the electrode at the formal potential of the redox couple. ^{14, 23, 25} They are more useful for probing the diamond films' electronic density of states over a large potential range.

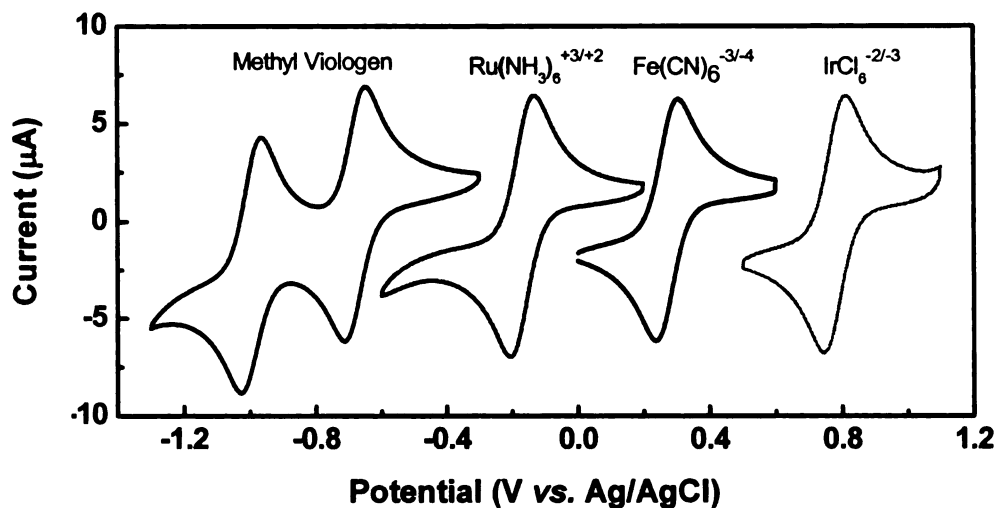


Figure 3-8 Cyclic voltammetric *i-E* curves for 0.1 mM Fe(CN)₆^{-3/-4}, methyl viologen, Ru(NH₃)₆^{+3/+2} and IrCl₆^{-2/-3}, all in 1 M KCl, at a diamond/Si OTE deposited for 4 h using 2 ppm B₂H₆. Scan rate = 0.1 V/s. Electrode geometric area = 0.2 cm².

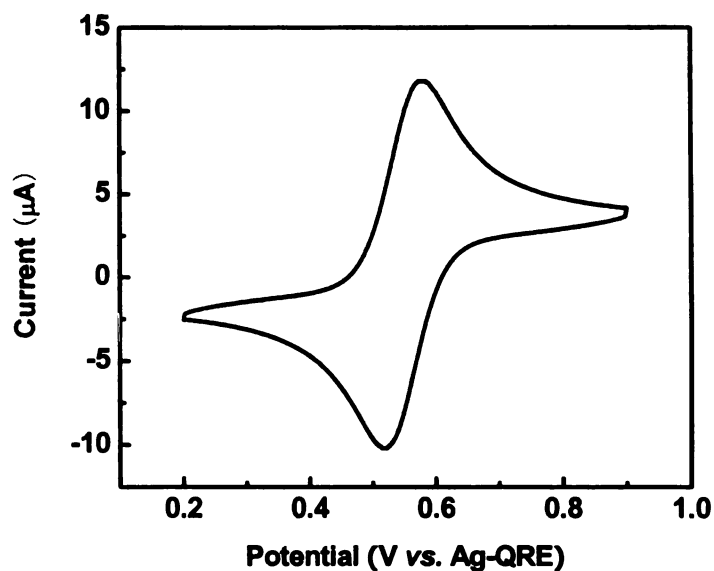


Figure 3-9 Cyclic voltammetric *i-E* curve for 0.1 mM ferrocene in 0.1 M TBABF₄/CH₃CN at a diamond/Si OTE deposited for 4 h using 2 ppm B₂H₆. Scan rate = 0.1 V/s. Electrode geometric area = 0.2 cm².

The reproducibility of the electrochemical responses was evaluated using five different diamond/Si OTEs. A summary of the data is presented in Table 3-3. ΔE_p for $\text{Fe}(\text{CN})_6^{-3/4}$ is 74 ± 6 mV (RSD = 8 %) at 0.1 V/s, suggesting the diamond/Si OTE has a clean, hydrogen-terminated surface. ΔE_p for methyl viologen, $\text{Ru}(\text{NH}_3)_6^{+3/+2}$ and $\text{IrCl}_6^{-2/-3}$ are 63 ± 3 mV (RSD = 5 %), 74 ± 6 mV (RSD = 8 %) and 65 ± 4 mV (RSD = 6 %), respectively, at 0.1 V/s. This observation suggests the diamond/Si OTE has a high density of electronic states over a wide range of potentials, sufficient to support rapid electrode-reaction kinetics. ΔE_p for ferrocene is 68 ± 9 mV (RSD = 13 %), indicating the diamond/Si OTE is active for a nonaqueous redox system. For all these redox systems, the forward scan peak current, i_p^{ox} , varied linearly with the scan rate^{1/2} between 50 and 500 mV/s. This indicates the reaction rate is limited by semi-infinite linear diffusion of the analyte to the surface. The $i_p^{\text{ox}}/i_p^{\text{red}}$ and $Q_p^{\text{ox}}/Q_p^{\text{red}}$ ratios were near 1.0 for these scan rates, as expected for a reversible system, and the values were stable with cycling.

Table 3-3 Summary of cyclic voltammetric data for diamond/Si OTEs deposited for 4 h using 2 ppm B_2H_6 . The scan rate was 0.1 V/s.

Redox system	ΔE_p (mV)	$E_{p/2}$ (mV)	i_p^{ox} (μA)	$i_p^{\text{ox}}/i_p^{\text{red}}$
$\text{Fe}(\text{CN})_6^{-3/4}$	74 ± 6	279 ± 2	6.2 ± 0.3	0.98 ± 0.01
Methyl viologen	63 ± 3	-681 ± 1	6.0 ± 0.1	1.01 ± 0.03
$\text{Ru}(\text{NH}_3)_6^{+3/+2}$	74 ± 6	-171 ± 1	6.8 ± 0.1	0.97 ± 0.01
$\text{IrCl}_6^{-2/-3}$	65 ± 4	777 ± 5	5.0 ± 0.1	1.00 ± 0.01
Ferrocene	68 ± 9	551 ± 5	11.7 ± 0.3	1.03 ± 0.02

In cyclic voltammetry, the applied potential is varied linearly with time. The faradaic peak current is given by

$$i_p = (2.69 \times 10^5) n^{3/2} A D^{1/2} C^* \nu^{1/2}$$

and the charging current, i_c , that always flows, is given by:²⁶

$$i_c = AC_d \nu$$

Combining these two equations yields the following ratio:

$$\frac{i_c}{i_p} = \frac{C_d \nu^{1/2}}{(2.69 \times 10^5) n^{3/2} D^{1/2} C^*}$$

A low C^* and high ν values, some distortion will occur to the wave shape as i_c becomes relatively more important. This effect will set the limit of *maximum useful scan rate and minimum useful concentration*.²⁶

Uncompensated ohmic resistances (R_u) in cyclic voltammetric experiment is manifested in large and distorted ΔE_p values for reversible redox couples. Ohmic resistance can originate from several sources: solution resistance, contact resistance, and electrode resistance. The solution resistance can be minimized by using a high concentration of supporting electrolyte and positioning the reference electrode as close to the working electrode as possible. We attempted to minimize the contact resistance by using graphite or Ag paste on the backside contact with the electrode. The electrode resistance is dominated by the boron-doping level.

The practical effect of R_u is to shift the reduction peak toward more negative potentials and the oxidation peak towards more positive potentials resulting in larger peak potential separations (ΔE_p). Since the current increases with C^* and $\nu^{1/2}$, the larger the concentration or the scan rate, the more E_p will be shifted if there is significant

uncompensated resistance. ²⁶ If ohmic resistance is significant, then ΔE_p will increase with the solution concentration of the redox molecule. If slow-electron transfer kinetics are dominating ΔE_p , then no change is expected with increasing analyte concentration.

Figure 3-10 shows cyclic voltammetric *i-E* curves for 0.05, 0.1, 0.5, and 1 mM $\text{Fe}(\text{CN})_6^{-3/-4}$, $\text{Ru}(\text{NH}_3)_6^{+3/+2}$, $\text{IrCl}_6^{-2/-3}$, and methyl viologen, all in 1 M KCl, at a diamond/Si OTE deposited for 4 h with 2 ppm B_2H_6 . The curves were recorded at 0.1 V/s. Table 3-4 summarizes the $i_{p,a}$ ($\text{Fe}(\text{CN})_6^{-3/-4}$) or $i_{p,c}$ ($\text{Ru}(\text{NH}_3)_6^{+3/+2}$, $\text{IrCl}_6^{-2/-3}$, and methyl viologen) and ΔE_p values for the redox systems at different concentrations. It is clear that ΔE_p for all the redox systems increases with increasing analyte concentration. Comparison measurements made with a diamond/Si electrode deposited for 10 h with 10 ppm B_2H_6 revealed an unchanging ΔE_p with increasing analyte concentration. ²⁷ The fact that ΔE_p increases for the lower doped diamond/Si OTE indicates the uncompensated resistance is associated with the electrode.

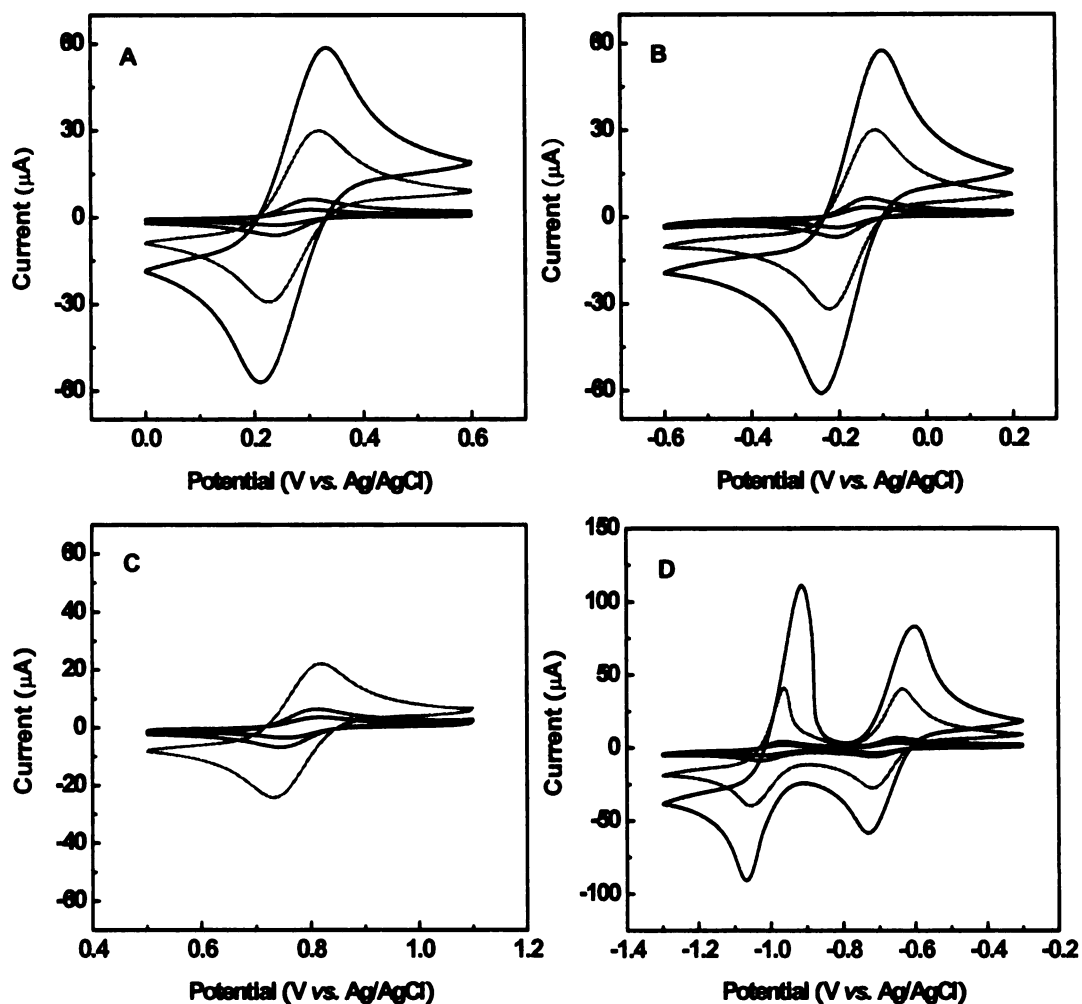


Figure 3-10 Cyclic voltammetric *i-E* curves for 0.05, 0.1, 0.5, and 1mM (A) $\text{Fe}(\text{CN})_6^{3-/4-}$, (B) $\text{Ru}(\text{NH}_3)_6^{+3/+2}$, (C) $\text{IrCl}_6^{-2/-3}$, and (D) methyl viologen, all in 1 M KCl, with a diamond/Si OTE deposited for 4 h with 2 ppm B_2H_6 . Scan rate = 0.1 V/s. Electrode geometric area = 0.2 cm^2 .

Table 3-4 Concentration dependence of the cyclic voltammetric data at a diamond/Si OTE.

Analyte	Concentration mM	$E_{p,a}$ mV	$E_{p,c}$ mV	ΔE_p mV	$i_{p,a}$ or $i_{p,c}$ μA
$\text{Fe}(\text{CN})_6^{-3/4}$	0.05	306	238	68	2.624
	0.1	306	239	67	6.525
	0.5	318	225	93	32.26
	1	332	209	123	62.45
$\text{Ru}(\text{NH}_3)_6^{+3/+2}$	0.05	-133	-203	70	3.495
	0.1	-132	-204	72	6.977
	0.5	-117	-222	105	33.85
	1	-101	-242	141	64.38
$\text{IrCl}_6^{-2/-3}$	0.05	816	754	62	3.411
	0.1	812	745	67	6.755
	0.5	821	733	88	24.85
MV	0.05	-651	-712	61	3.323
	0.1	-648	-713	65	6.128
	0.5	-636	-719	83	37.41
	1	-600	-731	131	79.67

Table 3-5 summarizes the $i_{p,a}$ ($\text{Fe}(\text{CN})_6^{-3/4}$) or $i_{p,c}$ ($\text{Ru}(\text{NH}_3)_6^{+3/+2}$, $\text{IrCl}_6^{-2/-3}$, and methyl viologen) and ΔE_p values for the redox systems at different scan rates in 0.1 mM $\text{Fe}(\text{CN})_6^{-3/4}$, $\text{Ru}(\text{NH}_3)_6^{+3/+2}$, $\text{IrCl}_6^{-2/-3}$, and methyl viologen, all in 1 M KCl, using a diamond/Si OTE deposited for 4 h with 2 ppm B_2H_6 . The scan rate was 0.1 V/s. Similarly, ΔE_p for each of the redox system was unchanged at low scan rates (< 0.1 V/s) and increased with increasing high scan rate.

Table 3-5 Scan rate dependence of the cyclic voltammetric data at a diamond/Si OTE.

Analyte	Scan rate V/s	$E_{p,a}$ mV	$E_{p,c}$ mV	ΔE_p mV	$i_{p,a}$ or $i_{p,c}$ μA
$\text{Fe}(\text{CN})_6^{-3/4}$	0.05	304	240	64	4.61
	0.1	306	239	67	6.525
	0.3	312	234	78	11.21
	0.5	316	230	86	14.24
$\text{Ru}(\text{NH}_3)_6^{+3/+2}$	0.05	-134	-204	70	4.911
	0.1	-132	-204	72	6.977
	0.3	-125	-213	88	11.96
	0.5	-119	-219	100	15.20
$\text{IrCl}_6^{-2/-3}$	0.05	811	746	65	4.721
	0.1	812	745	67	6.755
	0.3	817	741	76	11.82
	0.5	819	736	83	15.23
MV	0.05	-650	-713	63	4.260
	0.1	-648	-713	65	6.128
	0.3	-645	-717	72	11.17
	0.5	-638	-717	79	15.02

The concentration and scan rate dependence studies indicate that the uncompensated resistance (R_u) effects of the voltammetric response at the diamond OTE can be neglected at low concentrations (< 0.1 mM) and low scan rates (< 0.1 V/s).

3.3 Conclusions

Optically transparent boron-doped diamond film has been reproducibly deposited on an undoped silicon substrate using microwave-assisted chemical vapor deposition. Substrate pretreatment by mechanical polishing and complete cleaning introduces a high density of surface scratches and embedded diamond particles, with both functioning as initial nucleation sites for diamond growth. This is the key to the formation of a smooth

and continuous film in a short growth time. The deposition conditions were adjusted to maximize both the electrical conductivity and optical transparency.

The optical, physical, electrical and electrochemical properties of the diamond/Si OTE were described. SEM, Raman spectroscopy and XRD results confirm the presence of a thin, high quality boron-doped diamond film. The diamond/Si OTE transmits approximately 40-60% of IR light (2000-700 cm^{-1}). The film resistivity (0.1-0.4 $\Omega\text{-cm}$) is larger than the typical boron-doped polycrystalline films deposited on Si (0.01 $\Omega\text{-cm}$) previously reported on by our group.²⁸ This is due to a lower carrier concentration in the diamond/Si film due to a lower boron doping level. Even so, the resistivity is low enough to allow for relatively rapid electron-transfer reaction kinetics for several redox systems. The electrochemical properties were observed to be similar to those reported for high quality boron-doped diamond thin-film electrodes. This includes a wide working potential window of nearly 3 V in aqueous solution, a low and stable background current and good electrochemical responsiveness for aqueous $(\text{Fe}(\text{CN})_6)^{-3/4}$, methyl viologen, $\text{Ru}(\text{NH}_3)_6^{+3/+2}$ and $\text{IrCl}_6^{-2/-3}$, all in 1 M KCl) and nonaqueous (ferrocene in 0.1 M TBABF₄/CH₃CN) redox systems. These results further indicate that the diamond/Si OTE consists of a clean, mostly hydrogen-terminated sp^3 -bonded carbon surface, with no measurable contribution from the electrochemical signal by adventitious sp^2 -bonded carbon impurity or carbon-oxygen functional groups.

3.4 References

- (1) Zaitsev, A. M. *Optical Properties of Diamond*; Springer-Verlag: Berlin, 2001.
- (2) Ager III, J. W.; Walukiewicz, W.; McCluskey, M.; Plano, M. A.; Landstrass, M. I. *Appl. Phys. Lett.* **1995**, *66*, 616-618.
- (3) Clark, C. D.; Mitchell, E. W. J.; Parsons, B. J. In *The Properties of Diamond*; Field, J. E., Ed.; Academic: New York, 1979, pp 26-33.
- (4) McNamara, K. M.; Williams, B. E.; Gleason, K. K.; Scruggs, B. E. *J. Appl. Phys.* **1994**, *76*, 2466-2472.
- (5) Pankove, J. I.; Qiu, C. In *Synthetic Diamond: Emerging CVD Science and Technology*; Spear, K. E., Dismukes, J. P., Eds.; John Wiley & Sons: New York, 1994, pp 401-418.
- (6) Zhang, F.; Xie, E.; Yang, B.; Cai, Y.; Chen, G. *Mater. Lett.* **1994**, *19*, 115-118.
- (7) Ogasawara, A.; Inushima, T.; Shiraiishi, T.; Ohya, S.; Karasawa, S.; Shiomi, H. *Diam. Rel. Mater.* **1997**, *6*, 835-838.
- (8) Mort, J.; Machonkin, M. A.; Okumura, K. *Appl. Phys. Lett.* **1991**, *58*, 1908-1910.
- (9) Stotter, J.; Haymond, S.; Zak, J. K.; Show, Y.; Cvackova, Z.; Swain, G. M. *Interface* **2003**, *12*, 33-38.
- (10) Zak, J. K.; Butler, J. E.; Swain, G. M. *Anal. Chem.* **2001**, *73*, 908-914.
- (11) Stotter, J.; Zak, J.; Behler, Z.; Show, Y.; Swain, G. M. *Anal. Chem.* **2002**, *74*, 5924-5930.
- (12) Granger, M. C.; Swain, G. M. *J. Electroanal. Chem.* **1999**, *146*, 4551-4558.
- (13) Bennett, J. A.; Wang, J.; Show, Y.; Swain, G. M. *J. Electrochem. Soc.* **2004**, *151*, E306-E313.
- (14) Granger, M. C.; Witek, M.; Xu, J.; Wang, J.; Hupert, M.; Hanks, A.; Koppang, M. D.; Butler, J. E.; Lucazeau, G.; Mermoux, M.; Strojek, J. W.; Swain, G. M. *Anal. Chem.* **2000**, *72*, 3793-3804.
- (15) Enkevort, W. V. In *Synthetic Diamond: Emerging CVD Science and Technology*; Spear, K. E., Dismukes, J. P., Eds.; John Wiley & Sons: New York, 1994, pp 322-325.
- (16) Haymond, S. Ph. D. Dissertation, Michigan State University, East Lansing, 2002.

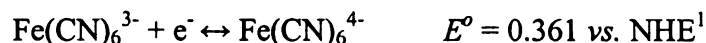
- (17) Yarbrough, W. A.; Messier, R. *Science (Washington, D. C., 1883-)* **1990**, *247*, 688-696.
- (18) Knight, D. S.; White, W. B. *J. Mater. Res.* **1989**, *4*, 385-393.
- (19) Ushizawa, K.; Watanabe, K.; Ando, T.; Sakaguchi, I.; Nishitani-Gamo, M.; Sato, Y.; Kanda, H. *Diamond and Related Materials* **1998**, *7*, 1719-1722
- (20) Gonon, P.; Gheeraert, E.; Deneuille, A.; Fontaine, F.; Abello, L.; Lucazeau, G. *Journal of Applied Physics* **1995**, *78*, 7059-7062.
- (21) Kinoshita, K., Ed. *Carbon: Electrochemical and Physicochemical Properties*; John Wiley & Sons: New York, 1988.
- (22) Bennett, J. Ph. D. dissertation, Michigan State University, East Lansing, MI, 2006.
- (23) Fischer, A. E.; Show, Y.; Swain, G. M. *Anal. Chem.* **2004**, *76*, 2553-2560.
- (24) Yagi, I.; Notsu, H.; Kondo, T.; Tryk, D. A.; Fujishima, A. *J. Electroanal. Chem.* **1999**, *473*, 173-178.
- (25) Show, Y.; Witek, M. A.; Sonthalia, P.; Swain, G. M. *Chem. Mater.* **2003**, *15*, 879-888.
- (26) Bard, A. J.; Faulkner, L. R. In *Electrochemical Methods: Fundamentals and Applications*, 2 ed.; John Wiley & Sons: New York, 2001, pp 228-238.
- (27) Wang, S.; Research Proposal, 2005.
- (28) Holt, K. B.; Bard, A. J.; Show, Y.; Swain, G. M. *J. Phys. Chem. B* **2004**, *108*, 15117-15127.

CHAPTER 4

IR Transmission Spectroelectrochemical Measurements With an Optically Transparent Boron-Doped Diamond Electrode

4.1 Introduction

As discussed in Chapter 1, IR spectroelectrochemistry is a useful technique for probing the molecular structure of reactants and products in redox reactions. In the work described herein, the redox system $\text{Fe}(\text{CN})_6^{-3/4}$ was used to evaluate the performance of the diamond OTE and the thin-layer transmission cell. This redox system undergoes a reversible, one-electron redox reaction:



This system is useful for mid-IR measurements because the CN vibrational frequency is sensitive to the oxidation state of the iron ($\text{Fe}(\text{CN})_6^{-3}$ ($\lambda_{\text{max}} = 2116 \text{ cm}^{-1}$) and $\text{Fe}(\text{CN})_6^{-4}$ ($\lambda_{\text{max}} = 2039 \text{ cm}^{-1}$)).

The main advantage of using a thin-layer cell design for spectroelectrochemical measurements is the short time required (typically 20-120 s) for complete electrolysis. This requires a cell with a large electrode area (A) to solution volume (V) ratio.² One method for achieving a large A/V ratio is to confine a very small volume (i.e., a few μL) into a thin layer ($< 100 \mu\text{m}$) adjacent to an electrode surface. As long as the solution thickness, l , is less than the diffusion layer thickness on the time scale of measurement,

$l \ll \sqrt{2Dt}$, finite diffusion will exist and the solution can be completely electrolyzed. For ideal thin-layer behavior, the cyclic voltammetric peak current, i_p , is equal to the following:

$$i_p = (9.39 \times 10^5) n^2 \nu V C_0^*$$

It can be seen that the peak current, varies linearly with the scan rate, ν , (V/s) and the analyte concentration, C (mol/cm³). The faradaic charge, Q , is independent of the scan rate according to the following expression:³

$$Q = nFN_0 = nFVC_0^*$$

From the faradaic charge, one can calculate the cell volume, V . The electrochemical performance of the thin-layer spectroelectrochemical cell was evaluated using these two relationships.

Thin-layer spectroelectrochemical studies are often conducted at a fixed potential. For a reversible system, the ratio of the concentration of the oxidized and reduced forms, $[Ox]/[Red]$, in the thin-layer cell is determined by the applied potential, E , according to the Nernst equation,

$$E = E^{o'} + \frac{0.059}{n} \log \frac{[Ox]}{[Red]}$$

In this expression, n is the number of electrons transferred per mole, and $E^{o'}$ is the formal reduction potential of the couple. The concentration of Ox and Red can be related to the absorbance through Beer's law:

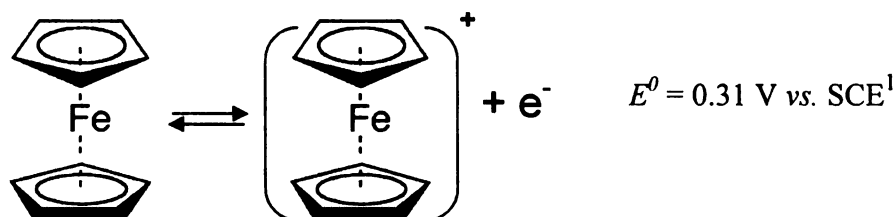
$$A = \epsilon b C .$$

In which, ϵ is the molar extinction coefficient ($M^{-1}cm^{-1}$), b is the optical pathlength (cm), and C is the analyte concentration (M). If the calculation is based upon one species, the molar extinction coefficient, ϵ , and the pathlength, b , can be cancelled:

$$E = E^{o'} + \frac{0.059}{n} \log \frac{A_{ox}}{A_{red}}.$$

One could generate a Nernst plot from the spectra at different potentials, from which the n and $E^{o'}$ can be extracted.

After characterizing the thin-layer transmission cell, the ferrocene/ferricenium redox couple was selected because of its usefulness in far-IR spectroelectrochemical measurements. This redox couple is routinely used as a model analyte in nonaqueous electrochemistry due to the highly reversible, well-behaved kinetic responses at a variety of electrode materials.^{2, 4} Ferrocene undergoes one-electron oxidation to the stable ferricenium cation:



Another reason for selecting this redox couple is the C-H bending modes perpendicular to the plane of the cyclopentadienyl ring in the far-IR region (ferrocene ($\lambda_{max} = 823\text{ cm}^{-1}$) and ferricenium ($\lambda_{max} = 857\text{ cm}^{-1}$)).⁵⁻⁷

Characterization of the diamond OTE in the thin-layer transmission cell with $Fe(CN)_6^{-3/4}$ and the ferrocene provided means for evaluating the performance of the diamond OTE in the mid- and far- IR. The far-IR work is a prerequisite for our future

studies that will involve investigating bonding interactions of the metalloproteins between the metal sites and their ligands in the far-IR ($< 1000 \text{ cm}^{-1}$).

4.2 Results and Discussion

Spectroelectrochemical measurements in the IR region were performed in the specially designed thin-layer cell, as described in Chapter 2. Characterization of the thin-layer cell was initially performed. Figure 4-1 (A) presents a background-corrected cyclic voltammetric i - E curve for 1 mM $\text{Fe}(\text{CN})_6^{4-}$ in 1 M KCl. A low potential scan rate of 1 mV/s was employed to minimize ohmic distortion of the voltammogram. As expected, the oxidation and reduction peak currents are approximately Gaussian in shape with no evidence of any diffusion or tailing. The i_p^{ox}/i_p^{red} ratio and Q_p^{ox}/Q_p^{red} ratio are both near 1. The i_p^{ox} value linearly with the scan rate ($R = 0.9999$) and the average of the oxidation and reduction peak potential, $E_{1/2}$, is 0.285 V. ΔE_p is 0.032 V, larger than the 0 V expected for ideal thin-layer behavior when the electrode kinetics are fast compared to the scan rate. The larger than expected ΔE_p is due to the ohmic resistance effects in the cell. The peak current increases linearly with the scan rate (oxidation current $R=0.9999$, reduction current $R=0.9998$), as shown in Figure 4-1 (B), while the faradaic charge is independent of the scan rate. From the average charge, $Q = 110 \text{ } \mu\text{C}$, the cell volume was calculated to be 1.14 μL according to $V = Q/nFC_{\text{bulk}}$. The volume calculated from the thin layer area (9.5 mm dia.) and thickness (7.5 μm) was 0.53 μL . The difference between the electrochemical volume and theoretical volume might due to the unevenly distributed spacer and the volume around the window.

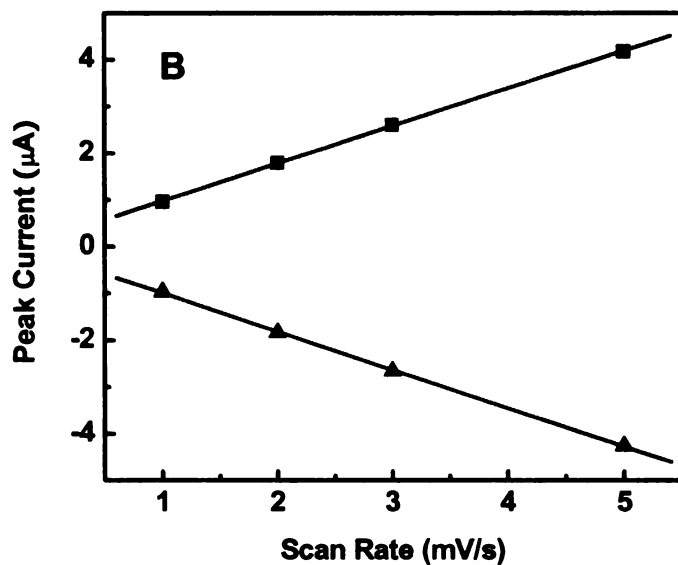
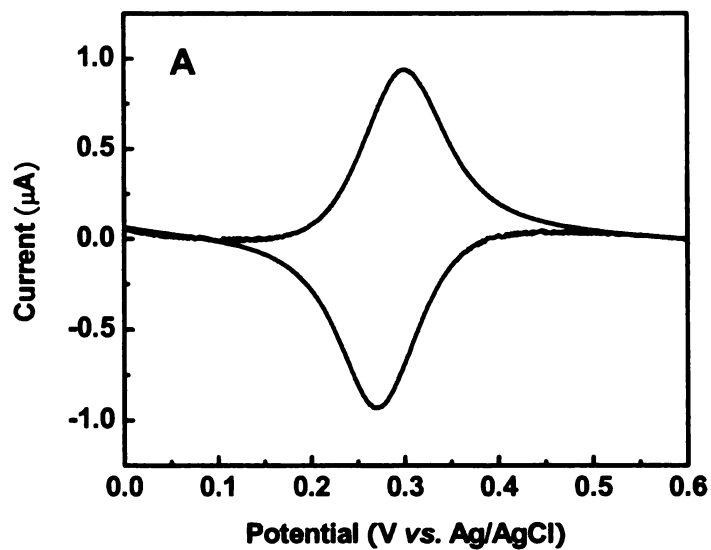


Figure 4-1 Cyclic voltammetric data for the diamond/Si OTE with 7.5 µm spacer. (A) Background-corrected thin-layer cyclic voltammetric *i-E* curve for 1 mM Fe(CN)₆⁴⁻ in 1 M KCl. The scan rate was 1 mV/s. (B) Plots of the oxidation (square) and reduction (triangular) peak current vs. scan rate for 1 mM Fe(CN)₆⁴⁻ in 1 M KCl. Data are shown for scan rates from 1 to 5 mV/s.

A series of difference absorbance spectra for 10 mM $\text{Fe}(\text{CN})_6^{4-}$ in 1 M KCl is presented in Figure 4-2. The potential was stepped from 0 (fully reduced) to values up to 0.50 V (fully oxidized) and a spectrum was collected 60 seconds after equilibration at each potential. The difference spectrum at each potential was generated by subtracting the reference spectrum obtained at 0 V for the fully reduced form of the couple. As the potential was stepped more positive, the oxidation of ferrocyanide to ferricyanide occurred. The positive-going peak at 2116 cm^{-1} is due to the $\text{Fe}(\text{CN})_6^{3-}$ generated in the cell. No changes in the absorbance spectra were seen beyond 0.5 V, indicating complete electrolysis of ferrocyanide. In good agreement with published data, the CN stretching mode at 2039 cm^{-1} shifts to 2116 cm^{-1} upon oxidation to ferricyanide.⁸⁻¹⁰ The molar extinction coefficients for these two transitions are obviously different. The greater the positive charge on the central metal, the less the metal can back bond electrons into π^* orbitals of CN ligands. The peak shift to the higher frequency for Fe^{+3} state means that there is less back bonding of metal electrons, a higher bond order and a larger CN bond energy.

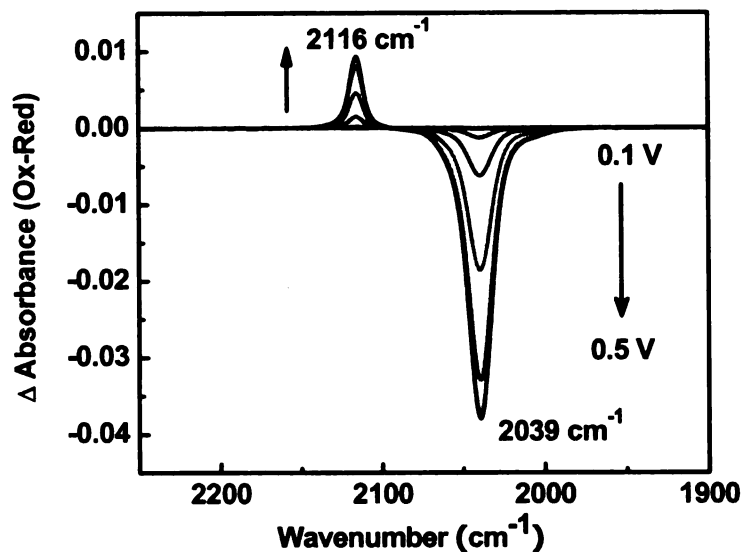


Figure 4-2 IR spectroelectrochemical difference absorbance spectra of $\text{Fe}(\text{CN})_6^{-3/4}$ at the diamond/Si OTE with a CaF_2 window. The optical pathlength was $7.5 \mu\text{m}$. The analyte solution was $10 \text{ mM Fe}(\text{CN})_6^{-4}$ in 1 M KCl . The potential was stepped from 0 to 0.1 V, 0.2 V, 0.25 V, 0.3 V, 0.35 V, 0.4 V, and 0.5 V vs. Ag/AgCl. Each spectrum was generated by subtracting the reference spectrum obtained at 0 V.

Combining the Nernst equation and Beer's law, a plot can be generated from the difference spectral data, that enables one to determine values of n and $E^{o'}$. The calculations can be based upon one species, then the molar extinction coefficient, ϵ , and the pathlength, b , are constant and can be cancelled. The modified Nernst equation is as follow:

$$E = E^{o'} + \frac{0.059}{n} \log \frac{A_{ox}}{A_{red}}$$

in which, $A_{ox} = \Delta A$, $A_{red} = A_{\text{max}} - \Delta A$

Where ΔA is the difference absorbance at a given potential, A_{max} is the maximum difference absorbance observed when $E_{\text{appl}} (>> E^{o'}) = 0.5 \text{ V}$.

Figure 4-3 presents Nernst plots for $\text{Fe}(\text{CN})_6^{-3/4}$ at two different wavenumbers. A linear relationship between the potential E and $\log (\Delta A_{\text{ox}}/\Delta A_{\text{red}})$ is seen for both indicating that equilibrium was reached and complete electrolysis occurred during the measurement. The $E^{\circ'}$ value of 0.294 V, determined from the y-axis intercept, is in good agreement with the value of 0.285 V obtained from cyclic voltammetry. The slope of the plot yields the number of electrons being transferred per mole in the redox reaction, in this case 1.

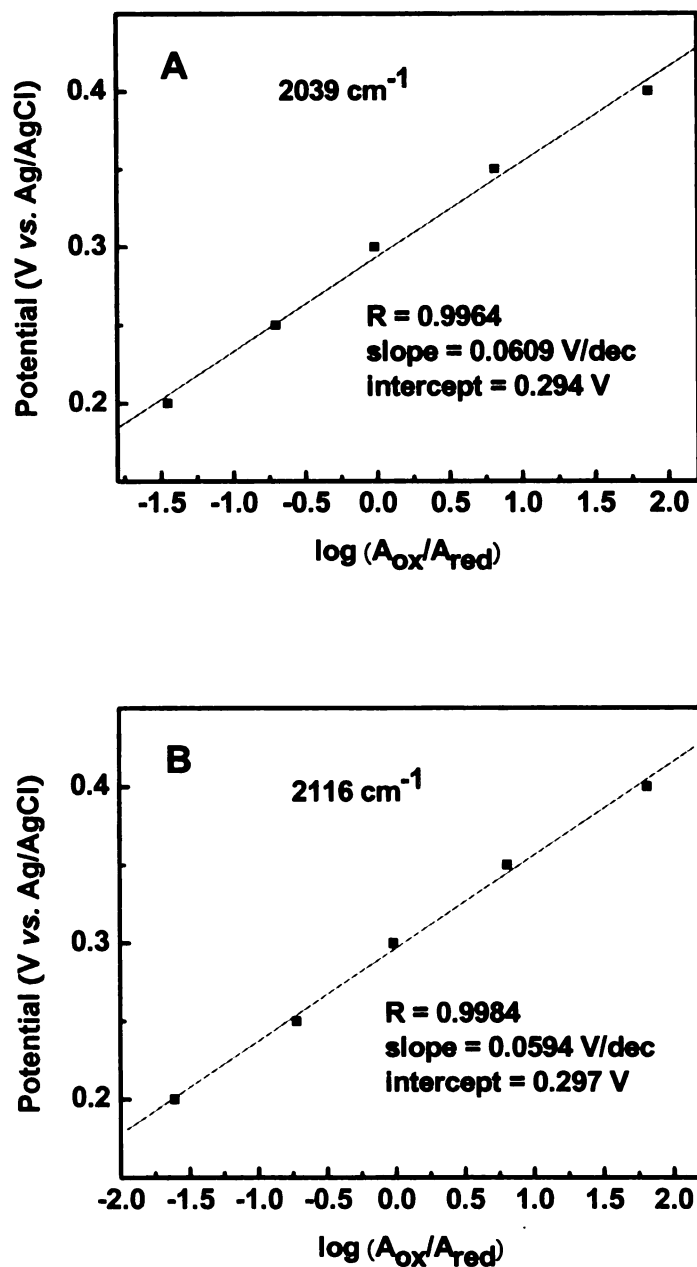


Figure 4-3 Nernst plots for 10 mM $\text{Fe}(\text{CN})_6^{4-}$ in 1 M KCl. (A) the $\text{Fe}(\text{CN})_6^{4-}$ absorption at 2039 cm^{-1} and (B) the $\text{Fe}(\text{CN})_6^{3-}$ absorption at 2116 cm^{-1} . Plots were generated from spectroelectrochemical data obtained with a diamond/Si OTE as presented in Figure 4-2.

Figure 4-4 shows the forward (oxidized minus reduced, dashed line) and reverse (reduced minus oxidized, solid line) IR difference absorbance spectra measured for 10 mM $\text{Fe}(\text{CN})_6^{4-}$ in 1 M KCl. The spectra were collected at 0.5 V and 0 V after 1 min equilibration time, respectively. The fact that these spectra are mirror images of one another indicates the reaction is reversible and complete with the thin-layer cell with little signal loss during the measurement in the custom-built cell.

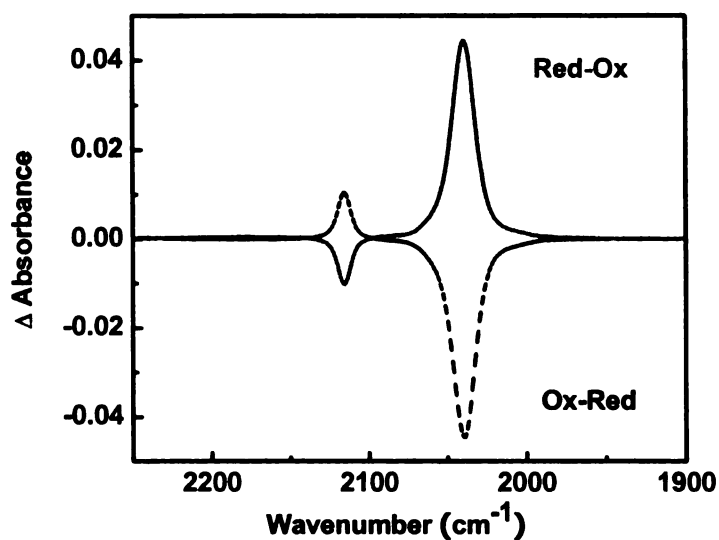


Figure 4-4 IR spectroelectrochemical absorbance spectra for $\text{Fe}(\text{CN})_6^{4-}$ (solid line) and electrogenerated $\text{Fe}(\text{CN})_6^{3-}$ (dashed line) at the diamond/Si OTE with a CaF_2 window. The optical pathlength was 7.5 μm . The analyte solution was 10 mM $\text{Fe}(\text{CN})_6^{4-}$ in 1 M KCl. Oxidized minus reduced (dashed line) and reduced minus oxidized (solid line) spectra were generated from the oxidized and reduced spectra collected at 0.5 and 0 V during a forward and reverse potential step for 60 s.

The absorbance-potential (voltabsorptometry) curve is another method for demonstrating complete electrolysis within the thin-layer cell.^{2, 11, 12} Figure 4-5 shows absorbance-potential curve recorded during one complete cyclic voltammetric cycle. The scan was initiated from 0 V and reversed at 0.6 V at a scan rate of 2 mV/s. Each point was determined from the absorbance intensity at the two wavenumbers recorded during 32 spectral scans from 2010 cm^{-1} to 2150 cm^{-1} at 4 cm^{-1} resolution. Since the IR spectra were collected over a range of wavenumbers during the scanning, the final difference absorbance at each potential was actually an average over a small range of potentials. There is no change in absorbance until 0.2 V at which point there are increases or decreases with measuring positive potential due to the oxidation of ferrocyanide to ferricyanide. Finally, a constant level is reached at potentials positive of 0.45 V. The reverse scan produces a near-mirror image of the forward scan with little hysteresis. The mirror images indicate that exhaustive electrolysis occurs in the cell and that the redox reaction is reversible. The full magnitude of the absorbance change at both wavenumbers is comparable with the data recorded during the potential step measurements shown in Figure 4-4.

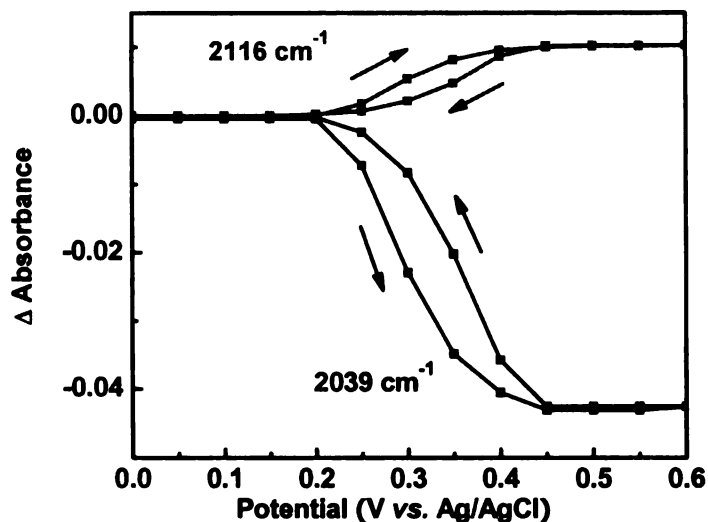


Figure 4-5 Difference absorbance-potential curves for $\text{Fe}(\text{CN})_6^{3-/4-}$ at the diamond/Si OTE with a CaF_2 window. The optical pathlength was $7.5 \mu\text{m}$. The measurement was made for a solution of $10 \text{ mM Fe}(\text{CN})_6^{4-}$ in 1 M KCl . The data were collected at a scan rate of 2 mV/s . The IR spectra were collected within a range of wavenumbers during the scanning, the final difference absorbance at each potential was actually an average of a small range of potential.

The potential-dependent thin layer far-IR difference spectra for 20 mM ferrocene in $0.1 \text{ M TBABF}_4/\text{CH}_3\text{CN}$ are presented in Figure 4-6. Similarly, the potential was stepped from 0.1 to 0.9 V in increments of 0.1 V and a spectrum was collected 60 seconds after equilibration at each potential. Each difference spectrum was generated by subtracting the reference spectrum obtained for the fully reduced form at 0.1 V from the spectrum obtained for the oxidation product at each potential. As the potential was stepped positive, a peak due to the C-H bending mode perpendicular to the plane of cyclopentadienyl ring of ferrocene at 823 cm^{-1} became more negative and the same mode for the ferricenium ion appeared at 857 cm^{-1} . The quantitative conversion of the redox couple is in good agreement with the results that have been reported.^{7,13} This experiment

is an important step toward our ultimate goal of applying the spectroelectrochemical method to measure the low-frequency ($< 1000 \text{ cm}^{-1}$) metal-ligand vibrations in metalloproteins.

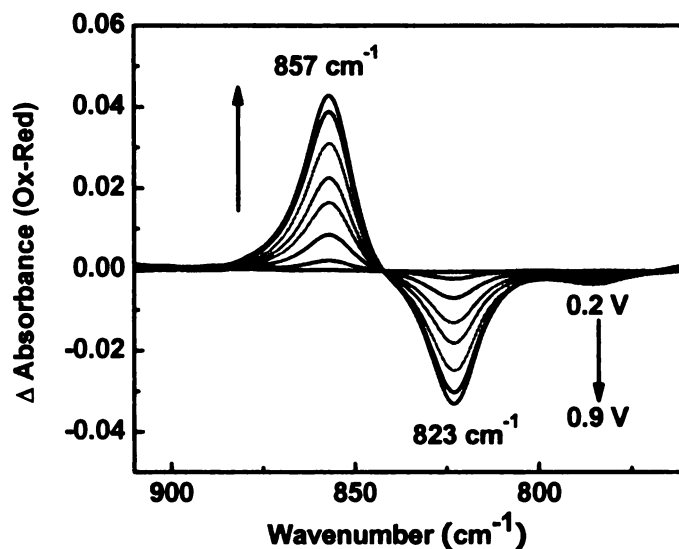


Figure 4-6 IR spectroelectrochemical difference absorbance spectra of ferrocene at the diamond/Si OTE with a Si window. The optical pathlength was $75 \mu\text{m}$. The analyte solution was 20 mM ferrocene in 0.1 M TBABF₄/CH₃CN. The potential was stepped from 0.1 to 0.9 V vs. Pt-QRE in increments of 0.1 V. Each spectrum was generated by subtracting the reference spectrum for the fully reduced form at 0.1 V.

4.3 Conclusions

The spectroelectrochemical performance of the diamond/Si OTE was evaluated in a new, custom-built transmission thin-layer cell. The OTE possessed good electrical conductivity and transparency for transmission spectroelectrochemical measurements. Well-behaved, thin-layer voltammetry was observed for the $\text{Fe}(\text{CN})_6^{-3/-4}$ redox couple with an i_p that increased linearly with scan rate and a Q that was independent of scan rate. The CN stretching vibration for ferrocyanide at 2039 cm^{-1} shifted to 2116 cm^{-1} upon

oxidation to ferricyanide in good agreement with the literature. A linear Nernst plot was observed with a slope of ca. 59 mV, consistent with 1 electron being transferred per mole of analyte. The observation of the perpendicular C-H bending mode shift from 823 cm^{-1} to 857 cm^{-1} showed the quantitative conversion of the ferrocene to the ferricenium ion. These results indicate that the thin layer cell design combined with the properties of the diamond/Si OTE enable rapid reproducible and quantitative spectroelectrochemical responses in the mid- and far- IR.

4.4 References

- (1) Bard, A. J.; Faulkner, L. R. In *Electrochemical Methods: Fundamentals and Applications*, 2 ed.; John Wiley & Sons: New York, 2001.
- (2) Haymond, S.; Zak, J. K.; Show, Y.; Butler, J. E.; Babcock, G. T.; Swain, G. M. *Anal. Chim. Acta* **2003**, *500*, 137-144.
- (3) Bard, A. J.; Faulkner, L. R. In *Electrochemical Methods: Fundamentals and Applications*, 2 ed.; John Wiley & Sons: New York, 2001, pp 228-238.
- (4) Haymond, S.; Babcock, G. T.; Swain, G. M. *Electroanalysis* **2003**, *15*, 249-253.
- (5) Lippincott, E. R.; Nelson, R. D. *Spectrochimica Acta* **1958**, *10*, 307-329.
- (6) Rosenblum, M. *Chemistry of the Iron Group Metallocenes: ferrocene, ruthenocene, osmocene*; Interscience: New York, 1965.
- (7) Lin, X.; Liu, Y.; Wang, E. *Acta Chimica Sinica* **1990**, *48*, 1080-1084.
- (8) Noguchi, T.; Inoue, Y. *J. Biochem.* **1995**, *118*, 9-12.
- (9) Pharr, C. M.; Griffiths, P. R. *Anal. Chem.* **1997**, *69*, 4673-4679.
- (10) Pharr, C. M.; Griffiths, P. R. *Anal. Chem.* **1997**, *69*, 4665-4672.
- (11) Niu, J.; Dong, S. *Electrochimica Acta* **1995**, *40*, 823-828.
- (12) Zak, J.; Porter, M. D.; Kuwana, T. *Anal. Chem.* **1983**, *55*, 2219-2222.
- (13) Ma, Y.; Zheng, J.; Zhu, S. *Journal of Inorganic Chemistry* **1999**, *15*, 61-67.

CHAPTER 5

Key Findings and Perspectives

5.1 Conclusions

The goal of the present work was to develop and characterize the new optically transparent boron-doped diamond thin-film deposited on undoped silicon. Such a material would be useful to elucidate structural changes in molecules associated with a change in the redox state using IR transmission spectroelectrochemical methods.

Chapter 3 demonstrated that optically transparent boron-doped diamond film can be reproducibly deposited on an undoped silicon substrate using microwave-assisted chemical vapor deposition. Detailed optical, physical, electrical and electrochemical properties of the diamond/Si OTE were described. The deposition conditions were adjusted to maximize both electrical conductivity and optical transparency. SEM, Raman spectroscopy and XRD results confirmed the presence of a thin, high quality boron-doped diamond film. The diamond/Si OTE transmits approximately 40-60% of IR light (2000-700 cm^{-1}). The low film resistivity (0.1-0.4 $\Omega\text{-cm}$) and good electrode activity produced relatively rapid electron-transfer reaction kinetics for several test redox systems. The electrochemical properties were found to be similar to those reported for high quality boron-doped diamond thin-film electrodes. These properties included a wide working potential window of nearly 3 V in aqueous solution, a low and stable background current and good electrochemical responsiveness for aqueous $(\text{Fe}(\text{CN})_6)^{-3/-4}$, methyl viologen,

$\text{Ru}(\text{NH}_3)_6^{+3/+2}$ and $\text{IrCl}_6^{-2/-3}$, all in 1 M KCl) and nonaqueous (ferrocene in 0.1 M TBABF₄/CH₃CN) redox systems. These results supported the notion that the diamond/Si OTE consists of a clean, mostly hydrogen-terminated sp³-bonded carbon surface, with no measurable contribution to the electrochemical signal from adventitious sp²-bonded carbon impurity or carbon-oxygen functional groups.

In Chapter 4, the mid- and far- IR spectroelectrochemical performance of the diamond/Si OTE in a new, custom-built transmission thin-layer cell was reported on. The initial testing with $\text{Fe}(\text{CN})_6^{-3/-4}$ solutions showed well-behaved thin-layer voltammetry, with an i_p that increased linearly with scan rate and a Q that was independent of scan rate. The CN stretching vibration mode for ferrocyanide at 2039 cm⁻¹ shifted to 2116 cm⁻¹ upon oxidation to ferricyanide in good agreement with the literature. A linear Nernst plot was observed with a slope of ca. 59 mV, consistent with 1 electron being transferred per mole of analyte. The observation of the C-H bending mode perpendicular to the plane of cyclopentadienyl ring of ferrocene shift from 823 cm⁻¹ to 857 cm⁻¹ showed the quantitative conversion of the ferrocene to the ferricenium ion. The results showed that the diamond/Si OTE possesses good electrical conductivity and optical transparency enabling rapid, reproducible and quantitative spectroelectrochemical measurements in the mid- and far- IR.

5.2 Future Research Directions

5.2.1 Metalloproteins

One-third of all proteins are "metalloproteins", which are chemical combinations of protein atoms (carbon, nitrogen, oxygen, hydrogen, sulfur) with metal ions such as iron, calcium, copper, and zinc. Hemoglobin, for example, that carries oxygen in the bloodstream, is an iron-containing metalloprotein. The metal ions in metalloproteins are critical to the protein's function, structure, and stability. In fact, numerous essential biological functions require metal ions, and most of the metal ion functions involve metalloproteins. Thus, metalloproteins make life on Earth possible and the ability to understand and ultimately control the binding and activity of protein metal sites is of great biological and medical importance.

Understanding the structure and function of metalloproteins requires knowledge of the structure and bonding at the metal center. These bonding interactions (e.g., M-OH, M=O, M-H₂O, etc) can be probed with mid- and far- IR electromagnetic radiation. Therefore, spectroelectrochemical measurements with the diamond/Si OTE have the potential to provide insight into the molecular structure of reaction intermediates and products in redox protein and enzyme processes. Future work will target several important metalloproteins: myoglobin, hemoglobin, cytochrome *c* and cytochrome *c* oxidase.

5.2.2 Far-IR Spectroelectrochemical Measurements of Redox Metalloproteins

There are a number of obstacles to making mid- and far-IR spectroelectrochemical measurements: strong water absorbance, limitations in the optical windows, detector sensitivity and temperature control problems. The broad water lattice vibrations below 1000 cm^{-1} are very sensitive to minute changes even for small pathlength ($6\text{ }\mu\text{m}$) or sampling conditions. The low signal-to-noise ratio because of the decreased light intensity in the far-IR region and the smaller vibrational mode extinction coefficients makes it hard to select the window material and detector with the right sensitivity. The baseline distortions due to the imprecise temperature control can result in the thermal bands. Each of these issues will be systematically addressed in future work.

MICHIGAN STATE UNIVERSITY LIBRARIES



3 1293 02956 1648